First geomorphological and sedimentological evidence for the combined tectonic and climate control on Quaternary Yarlung river diversion in the eastern Himalaya

Jin-Yu Zhang[1,2,*], An Yin[1,3,*], Wen-Can Liu[1,*], Lin Ding[4,*], and Xiao-Mei Xu[5,*]

[1]STATE KEY LABORATORY OF GEOLOGICAL PROCESSES AND MINERAL RESOURCES AND STRUCTURAL GEOLOGY GROUP, CHINA UNIVERSITY OF GEOSCIENCES, BEIJING 100083, P.R. CHINA
[2]INSTITUTE OF GEOLOGY, CHINA EARTHQUAKE ADMINISTRATION, BEIJING 100029, P.R. CHINA
[3]DEPARTMENT OF EARTH, PLANETARY, AND SPACE SCIENCES AND INSTITUTE OF PLANETS AND EXOPLANETS, UNIVERSITY OF CALIFORNIA, LOS ANGELES, CALIFORNIA 90095-1567, USA
[4]INSTITUTE OF TIBETAN PLATEAU RESEARCH, CHINESE ACADEMY OF SCIENCES, BEIJING 100101, P.R. CHINA
[5]DEPARTMENT OF EARTH SYSTEM SCIENCE, UNIVERSITY OF CALIFORNIA, IRVINE, CALIFORNIA 92697-3100, USA

ABSTRACT

This study investigates the combined effects of Quaternary climate change and tectonically induced topography on the Yarlung River drainage-system evolution in the eastern Himalaya. Our work integrates field mapping, geomorphological analysis, stratigraphy, sedimentology, optically stimulated luminescence dating, radiocarbon dating, and detrital-zircon dating of a Holocene valley-fill sequence in a Yarlung River tributary. This holistic approach reveals an aggradational event, which started at or soon after 24–20 k.y. B.P. and continued to or after 9.2–8.0 k.y. B.P. across the Himalayan drainage divide between the east-flowing Yarlung River in the north and the south-flowing Subansiri River in the south. The aggradational event was associated with a major phase of glacier advance during a period of warm and wet climate conditions in the eastern Himalaya; it was expressed by the deposition of a valley-fill sequence across the modern Yarlung-Subansiri drainage divide. South-flowing fluvial sediments across the divide and the elevation distribution of the fluvial terraces require the existence of a major glacier dam that either blocked a tributary or the main trunk of the Yarlung River. Although we are unable to differentiate the two competing scenarios, our work reveals that combined Holocene climate change and tectonically induced topography have played a major role in controlling rapid shifts in drainage geometry at a time scale of <10 k.y. across the Himalaya.

LITHOSPHERE; v. 8; no. 3; p. 293–316; GSA Data Repository Item 2016123 | Published online 5 May 2016 doi:10.1130/L500.1

INTRODUCTION

The Yarlung and Indus Rivers are the two dominant longitudinal (orogen-parallel) drainage systems flowing along the north side of the Himalaya (Burrard and Hayden, 1907) (Fig. 1A). The Yarlung River is the larger of the two, draining about a three-quarter length of the Himalayan range (Fig. 1A). At the eastern Himalayan syntaxis, the Yarlung River links with the Siang River, which cuts through the Himalaya and connects with the west-flowing Brahmaputra River in the Himalayan foreland (Fig. 1A). As the Yarlung-Siang-Brahmaputra River is the largest sediment-delivery system in the Himalaya and one of the largest in the world (Milliman and Meade, 1983; Ludwig and Probst, 1998), understanding its evolution has been an important part of continuing research with regard to the role of interactions among tectonics, surface processes, and climate change in shaping the topography and drainage-system evolution of the Himalayan orogen (e.g., Brookfield, 1998; Clark et al., 2004; Clift, 2006; Yin, 2006, 2010; Korup and Montgomery, 2008; Cina et al., 2009; Zhang et al., 2012; Lupker et al., 2013; Lang et al., 2013; Lang and Huntington., 2014; Wang et al., 2014).

Burrard and Hayden (1907) first suggested the Yarlung River to have episodically spilled over the Himalayan drainage divide as a result of tectonic blockage. They also postulated the Yarlung River to have originally linked with the Indus River flowing westward; this was followed by reversing the flow direction along the eastern segment of the ancestral Indus-Yarlung River that first flowed across southern China and then achieved the modern configuration of the Yarlung River by flowing through the eastern Himalayan syntaxis. Following their pioneering work, researchers have inferred that (1) the Yarlung River is antecedent to the Himalayan topography and its course has remained stationary since at least early Miocene time (e.g., Burg et al., 1998; Hallet and Molnar, 2001; Seward and Burg, 2008; Lang and Huntington, 2014; Bracciali et al., 2015), or (2) the river recently flowed (a few m.y. to <15 m.y. ago) along the Lohit (Seeber and Gornitz, 1983), Irrawaddy (Brookfield, 1998; Zeitler et al., 2001; Clark et al., 2004; Liang et al., 2008), or Subansiri (Cina et al., 2009; Zhang et al., 2012; Robinson et al., 2013) Rivers before establishing its current course.

With the exception of Cina et al. (2009) and Zhang et al. (2012), we are not aware of any work that has addressed the question of when and how the Yarlung River was diverted across the Himalaya as originally envisioned by Burrard and Hayden (1907) more than 100 years ago. Based on the paleocurrent data and the high percentage of Jurassic to early Tertiary detrital zircon in the Upper Miocene and Pliocene strata in the eastern Himalayan foreland basin, Cina et al. (2009) proposed that the Yarlung River was once linked with the south-flowing paleo–Subansiri River between 11 Ma and 5 Ma; the connected paleo–Yarlung-Subansiri River was

*Zhang—jinyuzhang86@gmail.com; Yin, corresponding author—yin@ess.ucla.edu, ayin54@gmail.com; Liu—liuwenc@cugb.edu.cn; Ding—dinglin@itpcas.ac.cn; Xu—xxu@uci.edu.

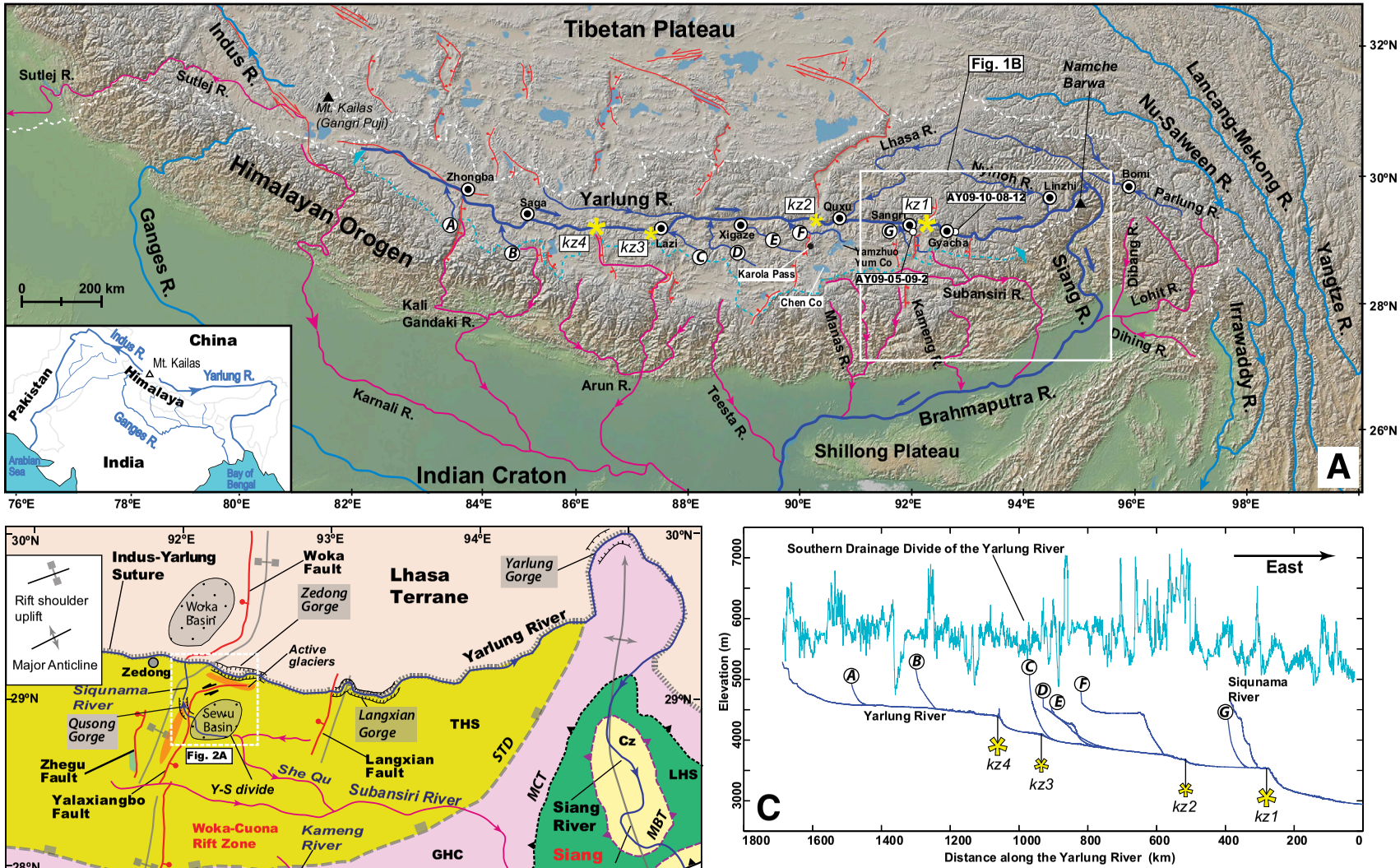

Figure 1. (A) A shaded relief map showing the distribution of major drainage systems and active structures across the central and eastern Himalaya. The inset map shows the context of the major longitudinal rivers in the Himalaya. The drainage divides of the Indus, Ganges, and Yarlung drainage basins are marked by white dashed lines except a portion of the Yarlung southern divide in light blue that marks the topographic profile shown in C. Also shown are locations of four major knickzones along the Yarlung River (yellow snowflake symbols and marked as kz1 to kz4). The detrital-zircon sand samples from the Yarlung River near Gyacha and the Siqunama River (i.e., AY09-10-08-12 and AY09-05-09-2 of Zhang et al., 2012) are also marked by white circles. Digital topographic map was derived from the Global Multi-Resolution Topography (GMRT) Synthesis by Ryan et al. (2009) (http://www.geomapapp.org). (B) Simplified tectonic map of the eastern Himalayan orogen modified from Yin et al. (2010) and Burg et al. (1998). Y-S divide—Yarlung-Subansiri drainage divide; MCT—Main Central thrust; MBT—Main Boundary thrust; MFT—Main Frontal thrust; TT—Tipi thrust; STD—South Tibet detachment; THS—Tethyan Himalayan Sequence; LHS—Lesser Himalayan Sequence; GHC—Greater Himalayan Crystalline Complex; Cz—Cenozoic strata. (C) Longitudinal profiles for the Yarlung River and its southern tributaries west of 94°E and the elevation of the southern Yarlung River divide. Four knickzones corresponding to those shown in A are also indicated along the Yarlung River longitudinal profile.

sourced from southern Tibet north of the Indus-Yarlung suture, allowing it to deliver 200–50 Ma Gangdese-arc detrital zircon to the Himalayan foreland. This interpretation was disputed by Lang and Huntington (2014) based on a study of detrital-zircon ages at sites ~300 km east of Cina et al.'s (2009) study area. However, the lack of paleocurrent and sedimentological studies from the sample sites of Lang and Huntington (2014) makes their inferred zircon provenance and paleo–Yarlung River geometry ambiguous.

A fundamental obstacle in resolving whether the Yarlung River has changed its course in the past 15–10 m.y. is the lack of direct evidence of the linkage between the Himalayan longitudinal and transverse rivers. Considering the fact that the eastern Himalaya has experienced >5–10 km of crustal denudation since ca. 15 Ma (Grujic et al., 2006; Yin et al., 2010; Adlakha et al., 2013; McQuarrie and Ehlers, 2015; Adams et al., 2015), the morphologic and related sedimentological records of the inferred river (i.e., a linked longitudinal-transverse river flowing over the Himalayan crest) must have been erased. To resolve this issue we investigated the Quaternary geomorphologic and sedimentologic evolution of a Quaternary valley-fill sequence across a segment of the Yarlung-Subansiri divide in the eastern Himalaya (Fig. 1A). Our work, combining field mapping, stratigraphic measurements, sedimentologic analyses, Quaternary age dating, geomorphological investigation, and detrital-zircon dating, shows that the aggradational event leading to the deposition of the studied valley-fill sequence started at or after 24–20 k.y. B.P. and was ongoing until or after 9.2–8 k.y. B.P. The aggradational event was closely associated with rapid advance of alpine glaciers, which was followed by the deposition of a south-flowing fluvial sequence across the modern drainage divide between the east-flowing Yarlung River in the north and the south-flowing Subansiri River in the south. The results of our work help illuminate the proposed spillover and antecedent processes for the drainage evolution in the eastern Himalaya (Cina et al., 2009; Lang and Huntington, 2014; Bracciali et al., 2015).

GEOLOGICAL FRAMEWORK

Tectonic Setting

The study area, located south of the Indus-Yarlung suture zone across the northern flank of the Himalayan range, is a rift-bounded basin (Fig. 1B). The suture zone, followed roughly by the Yarlung River, is marked by the Oligo-Miocene south-dipping Renbu-Zedong thrust, which juxtaposes Triassic flysch deposits, part of the Proterozoic-Eocene Tethyan Himalayan Sequence, over the Jurassic–early Tertiary Gangdese granitoids of the southern Lhasa terrane (Yin et al., 1994, 1999; Harrison et al., 2000; Yin et al., 2006, 2010) (Fig. 1B). High-grade metasedimentary rocks (i.e., quartzite, schist, gneiss, and meta-granitoids of the Tethyan Himalayan Sequence basement) and ca. 42 Ma granitoids are exposed in the Yalaxiangbo gneiss dome (Fig. 2A) (Zeng et al., 2011). The dominantly isoclinally folded Tethyan Himalayan Sequence strata are intruded by the undeformed ca. 44 Ma Dala granitoid directly south of our study area (Aikman et al., 2008, 2012a, 2012b). The 40–45 Ma Yalaxiangbo and Dala granitoids overlap in age to the youngest phase of magmatism in the Gangdese batholith north of the suture (e.g., Zhang et al., 2012).

Active tectonics in the study area is expressed by the development of the north-trending Woka-Cuona rift zone (e.g., Armijo et al., 1986; Yin, 2000; Taylor et al., 2003; Yin, 2010), which cuts and offsets the Main Central Thrust exposed in the southern flank of the Himalaya (Yin et al., 2010) (Fig. 1B). North of the Yarlung River the west-dipping Woka fault bounds the Woka rift basin, whereas south of the Yarlung River the east-dipping Yalaxiangbo fault bounds the Sewu basin that is the focus of this study. The oppositely dipping Yalaxiangbo and Woka faults turn from a north strike to an east strike as they approach one another near the Yarlung River (Fig. 1B), which is possibly caused by a change in the mechanical properties of the crust north and south of the Indus-Yarlung suture (Yin, 2000).

A north-trending ridge, reaching >6700 m in elevation through the Yalaxiangbo dome (glaciated area III in Fig. 2A), lies along the west side/footwall of the Yalaxiangbo fault. Apatite fission-track dating indicates that the Yalaxiangbo footwall has been rapidly exhumed since ca. 4 Ma (Zhao et al., 2003). The region between the east-striking southernmost Woka fault and the east-striking northernmost Yalaxiangbo fault is a 40-km-long east-trending horst with glacier-covered peaks reaching >5500 m in elevation (glaciated areas I and II in Fig. 2A). The Yarlung River cuts through this fault-bounded high ridge and forms a spectacular river gorge that is 2 km high and <1 km wide at its narrowest segment. The Gangdese granitoids comprise the steep north wall, whereas the low-grade Tethyan Himalayan rocks comprise the steep south wall of this gorge (Yin et al., 1994, 1999). The gorge is hereafter referred to as the Zedong Gorge.

Drainage Systems

The major drainage systems examined in this study are the longitudinal Yarlung River and the transverse Subansiri River (Fig. 1B). The Yarlung River makes a tight 180° hairpin loop around the eastern Himalayan syntaxis and becomes the south-flowing Siang River. At the eastern syntaxis, the Yarlung River forms a deep-cut gorge commonly referred to as the Yarlung Gorge. The lowest elevations of the southern drainage divide of the Yarlung River is ~5750 m west of ~90°E and <5000 m east of this longitude (Figs. 1A and 1C). Major Yarlung tributaries (A to G in Fig. 1A) across the north flank of the Himalaya are significantly shorter (<200 km) than transverse rivers across the south flank of the Himalayan range (generally >400–500 km). Four major knickzones have been identified along the Yarlung River (yellow markers in Figs. 1A and 1C), all located at or near the intersection of the Yarlung River and major active north-trending rift zones (Zhang, 2001). These knickzones may either be created by rift-related normal faulting (Zhang, 2001) or by wave-like migration of knickzones that started from the Yarlung Gorge at the eastern Himalayan syntaxis and were "arrested" by the rift zones (Schmidt et al., 2015). One knickzone (Zedong knickzone) is associated with a deep-cut gorge flanked by >5000 m glaciated peaks and controlled by the Woka-Yalaxiangbo normal fault system (i.e., the Zedong Gorge referred in this study; see Fig. 1B). The north-flowing Siqunama River, along which this study was conducted, is located directly west of this knickzone (Fig. 1C).

The Zedong knickzone separates a braided-stream-channel segment of the Yarlung River in the west from a meandering-stream-channel segment of the Yarlung River in the east (Figs. 2B and 2C). This change in the stream channel form is most likely induced by a higher sediment supply, possibly from the Lhasa River, west of the knickzone than that in the east (e.g., Schumm and Khan, 1972), as the river segments share a similar longitudinal gradient (Fig. 1C). The Subansiri River, the second longest river after the Yarlung River in the eastern Himalaya (Fig. 1B), displays an unusual pattern among the Himalayan transverse rivers in that its headwater streams extend >200 km north of the Himalayan crest. There, the main trunk of the Subansiri River flows parallel to the strike of the Himalaya and its divide against the Yarlung drainage basin is located north of the high peaks of the Himalaya and within 40 km from the main trunk of the Yarlung River (Fig. 1B).

Our study area is located along a segment of the Yarlung-Subansiri drainage divide, where the Siqunama River flows northward into the main trunk of the Yarlung River and the She Qu (Qu means small stream in Tibetan) flows eastward and then southward into the main trunk of the Subansiri River (Fig. 2A). The

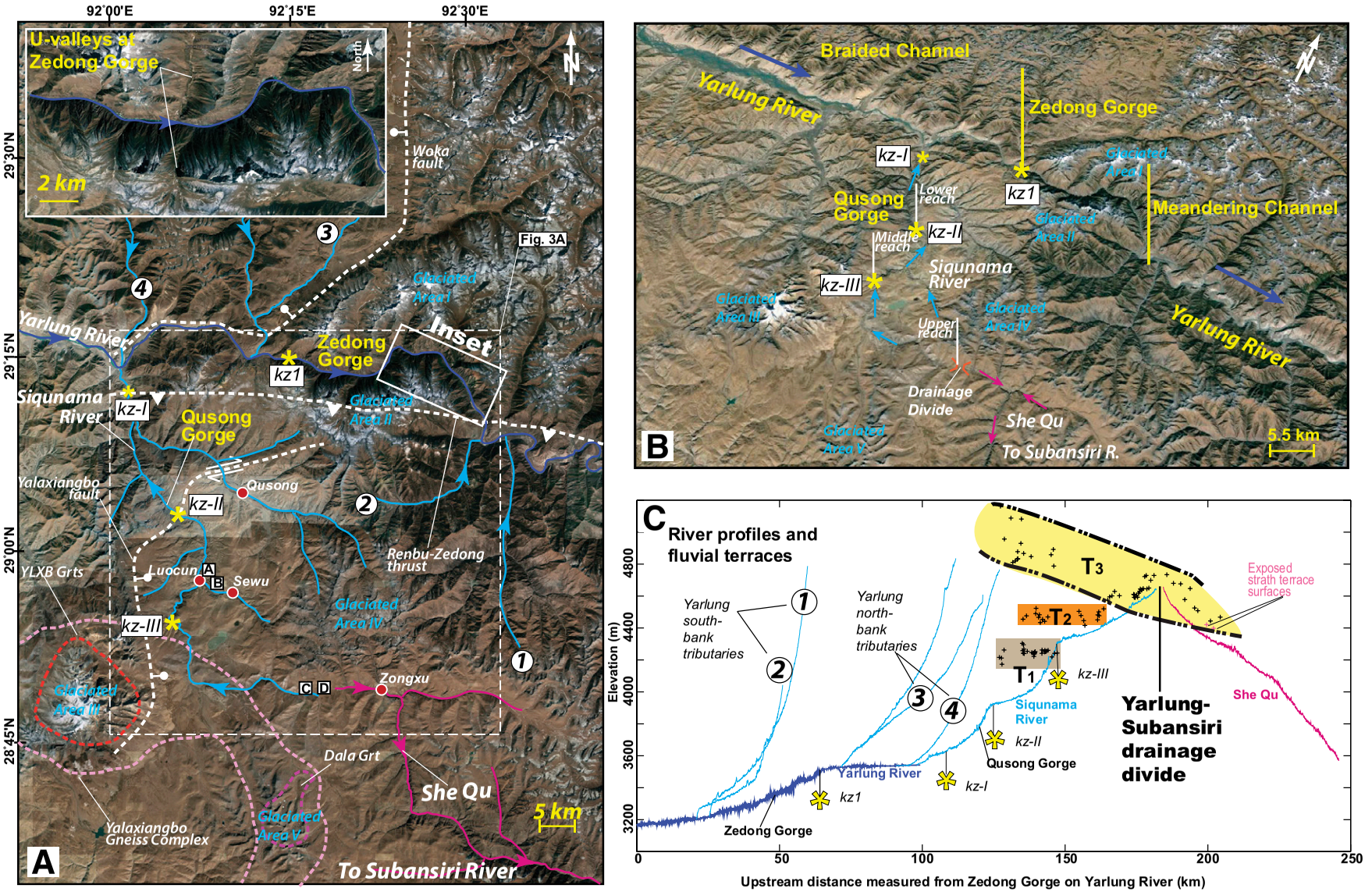

Figure 2. (A) Google Earth image showing the locations of major drainages, glacier-covered high mountainous regions, and knickzones in of the study area. Letters A to D are locations of U-Pb detrital-zircon samples collected in this study. Inset map is an oblique Google Earth image showing hanging valleys on the two sides of the Zedong Gorge. Abbreviations: YLXB Grts—Yalaxiangbo gneiss complex and related granitoids; Dala Grt—Dala granitoid. Inset figure shows the location of Figure 3A. (B) An oblique Google Earth image that shows changes of channel geometry west and east of the Zedong Gorge along the Yarlung River. Also shown is a change in morphology along the upper, middle, and lower reaches of the Siqunama River. No longitudes and latitudes are labeled as this is an oblique view. (C) Longitudinal profiles of the Yarlung River, Siqunama River, and She Qu and locations of major knickzones. Scattered cross symbols represent the elevation distributions of three levels of fluvial terraces exposed along the Siqunama–She Qu river valleys. The elevation data are derived from Shuttle Radar Topography Mission 30 m digital elevation model.

Siqunama–She Qu divide lies at an elevation of ~4760 m, which is ~1200 m above the elevation of the Yarlung River at the Zedong Gorge (Fig. 2A). The Siqunama River originates from glaciated mountains (Glaciated Areas III, IV, and V in Figs. 2A and 2B) and can be divided into three segments bounded by two knickzones at ~4320 m and ~3950 m, respectively (kz-III and kz-II in Fig. 2C). The upper reach is dominated by U-shaped glacial valleys and kettle lakes as a result of glacial retreat. The middle reach displays V-shaped and deep-cut (>200 m in places) fluvial valleys, locally associated with meandering-stream channels on top of Quaternary alluvial deposits. The lower reach cuts through a narrow bedrock gorge composed of Triassic meta-sedimentary strata. This gorge is referred to as the Qusong Gorge in this study (Fig. 2A). The Qusong Gorge is located along the active trace of the Yalaxiangbo normal fault.

The She Qu and four additional tributaries of the Yarlung River in the study area, labeled as streams (1) to (4) in Figures 2B and 2C, do not display discernable knickzones along their longitudinal profiles. Unlike the Siqunama River, we note that the aforementioned streams do not cut across active faults. Thus, it appears that the knickzones along the Siqunama River were tectonically induced.

Fluvial Terraces

South of the Zedong Gorge. Three levels of fluvial terraces are recognized along the Siqunama River in the hanging wall of the Yalaxiangbo fault (Figs. 3A–3C). The elevation distribution of the terraces and their relative heights to the Siqunama stream channel are shown in Figure 2C. The highest terrace T_3 is expressed as discontinuous but laterally correlative bench-like flat surfaces, which cut into Triassic bedrock at elevations of 4750–4800 m (Figs. 2C and 3D). Fluvial deposits associated with T_3 are generally absent except at the Yarlung-Subansiri divide (i.e., the headwaters of the Siqunama River and She Qu), where terrace treads are located >50 m above the Siqunama River–She Qu divide. We interpret T_3 as a fill terrace generated during the peak of an aggradational event. The lower fluvial terraces of T_2 and T_1 are fill-cut terraces developed along both sides of the Siqunama River at ~4400–4500 m and ~4200–4300 m, respectively (Figs. 2C, 3A, and 3D).

North of the Zedong Gorge. We conducted reconnaissance work only in areas immediately north of the Zedong Gorge along the Woka rift basin (Fig. 4). Our observations described below are mostly based on the analysis of Google Earth images and field observations at the southern end of the rift basin against the Yarlung River. Our efforts reveal the presence of three levels of subhorizontal geomorphological surfaces that are interpreted as treads of fluvial/lacustrine terraces (Fig. 4). These terraces lie at the elevation of 4100–4300 m, 4450–4500 m, and 4750–4900 m, respectively, which correlates remarkably well with the elevations of the three levels of major terraces exposed in the Siqunama drainage basin south of the Yarlung River (cf. Fig. 3). The elevation correlation of the terraces north and south of the Yarlung River suggests that their formation was probably induced by the same sequence of aggradation and degradation associated with the expansion and shrinking of the Yarlung River basin west of the Zedong Gorge.

A series of hanging valleys filled by active debris-rich glaciers lie at an elevation of ~4700–4800 m above the Woka normal fault scarp (Fig. 4). This morphological feature suggests that glaciers once filled up the fault-bounded Woka basin to an elevation as high as >4700 m. This situation is similar to the well-documented case along the famed Yosemite Valley in the western United States (Matthes, 1972), where glaciers with a thickness of >1300 m were once present in the valley. Glacier jamming at the Zedong Gorge would imply the formation of an ice dam along the Yarlung River. This inference is consistent with the presence of hundreds of dissected Quaternary ice dams along the Yarlung River (e.g., Korup et al., 2010). In fact, one such ice dam is located at the western edge of the Zedong Gorge where the north-trending Woka basin intersects the Yarlung River (Fig. 4) (Korup et al., 2010). At the site of this inferred ice dam are glacial-wash deposits consisting dominantly of granitic boulders that are cut by the lowest terrace surface at an elevation of ~4300 m north of the Yarlung River (Fig. 5). This terrace surface is ~500 m above the elevation of the current Yarlung River channel. The presence of moraine deposits at this site is consistent with it being jammed by glacier/glacial deposits, but the cross-cutting relationship with the younger terrace indicates that the ice dam has been strongly modified; the original height of the ice dam must have been higher than its current elevation as indicated by the preserved fluvial terraces.

It is interesting to note that the basal elevation of the U-shaped hanging valleys along the two sides of the Zedong Gorge is similar to the elevation of the highest terrace tread in the Woka basin. Although this correlation may suggest that the formation of the two geomorphic features may have been genetically related, two factors must have altered the elevation of the hanging valleys with time in the footwall of the Woka fault: (1) down-cutting erosion by the moving glaciers in the hanging valleys after the deposition of the aggradational sequence in the Woka Valley, and (2) upward motion by normal faulting along the Woka normal fault. For temperate valley glaciers such as those in southern Tibet and the eastern Himalaya, its erosional rate is typically in the range of 1–10 mm/yr (Hallet et al., 1996). East-west extension across Tibet is ~20 mm/yr as determined by global positioning system (GPS) measurements (Zhang et al., 2004), which is distributed over 7 major rifts (Taylor and Yin, 2009). Assuming that the extension is evenly distributed across each rift in southern Tibet, a 3 mm/yr extension rate is required across the Woka fault. This would result in a vertical velocity of ~5.2 mm/yr for the footwall motion along a 60°-dipping normal fault. As this tectonically induced uplift rate is comparable in magnitude to the erosion rate by glaciers, the hanging wall valley may have maintained a similar elevation in the Holocene assuming that both the GPS and glacier erosion rates based on modern observations have been constant in the late Quaternary.

STRATIGRAPHY AND SEDIMENTOLOGY

Stratigraphic Division

A sequence of >250-m-thick valley fill, consisting of clay, silt, sand, gravel, and diamicton, is mapped across the Siqunama drainage basin and the headwater region of the She Qu linking with the Subansiri River (Figs. 3A and 5). The sequence lacks prominent erosional surfaces and unconformities and is therefore interpreted as a result of a single and continuous aggradational event. The valley-fill strata can be divided into the lower, middle, and upper members based on their distinctive lithology and sedimentary structures (Figs. 5 and 6A).

The cliff-forming lower member (Unit 1) is dominated by clast-supported massive to crudely layered fine-grained (3–6 cm) gravels with well-developed imbrication structures. Within the gravel beds are sand lenses (tens of centimeters thick and 1–5 m long) that display either horizontal bedding or planar cross-bedding (Fig. 6B). The gravel beds are typically 3–5 m thick and are bounded by sheet-like coarse-grained and gravelly sand beds that can be traced tens to >100 m laterally. As the sheet-like sand layers are less resistant to weathering than the gravel layers, Unit 1 displays a distinctive semi-rhythmic outcrop pattern in deep-cut river-channel walls (Fig. 6A).

The slope-forming middle member (Unit 2) consists of massive clay and pebbly silt with rare layering (Fig. 6C). Peats are present in the pebbly silt and were collected for radiocarbon dating (see details below). The sedimentary fines

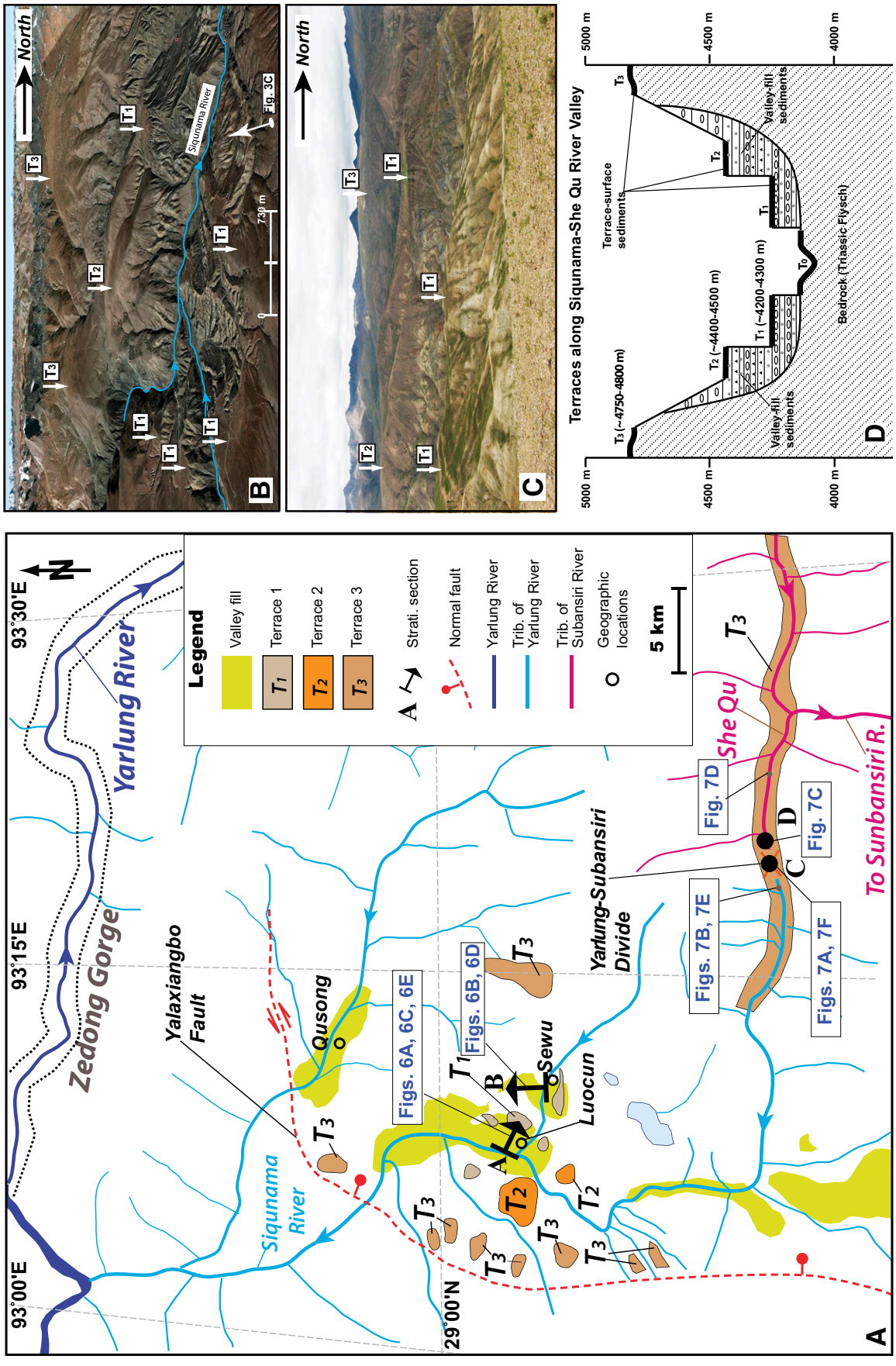

Figure 3. (A) Distribution of valley-fill sediments and fluvial terraces along the Siqunama and She Qu river valleys. Locations of measured stratigraphic sections A, B, C, and D in Figure 5 are also shown. Locations of field pictures shown in Figures 6 and 7 are indicated in the map. (B) Perspective view of fluvial terraces along the Siqunama River from Google Earth. (C) Field picture of fluvial terraces developed along the western side of the Siqunama River. (D) Sketch map illustrating the averaged elevations of three fluvial terraces and their relationships to valley-fill sediments along the Siqunama River.

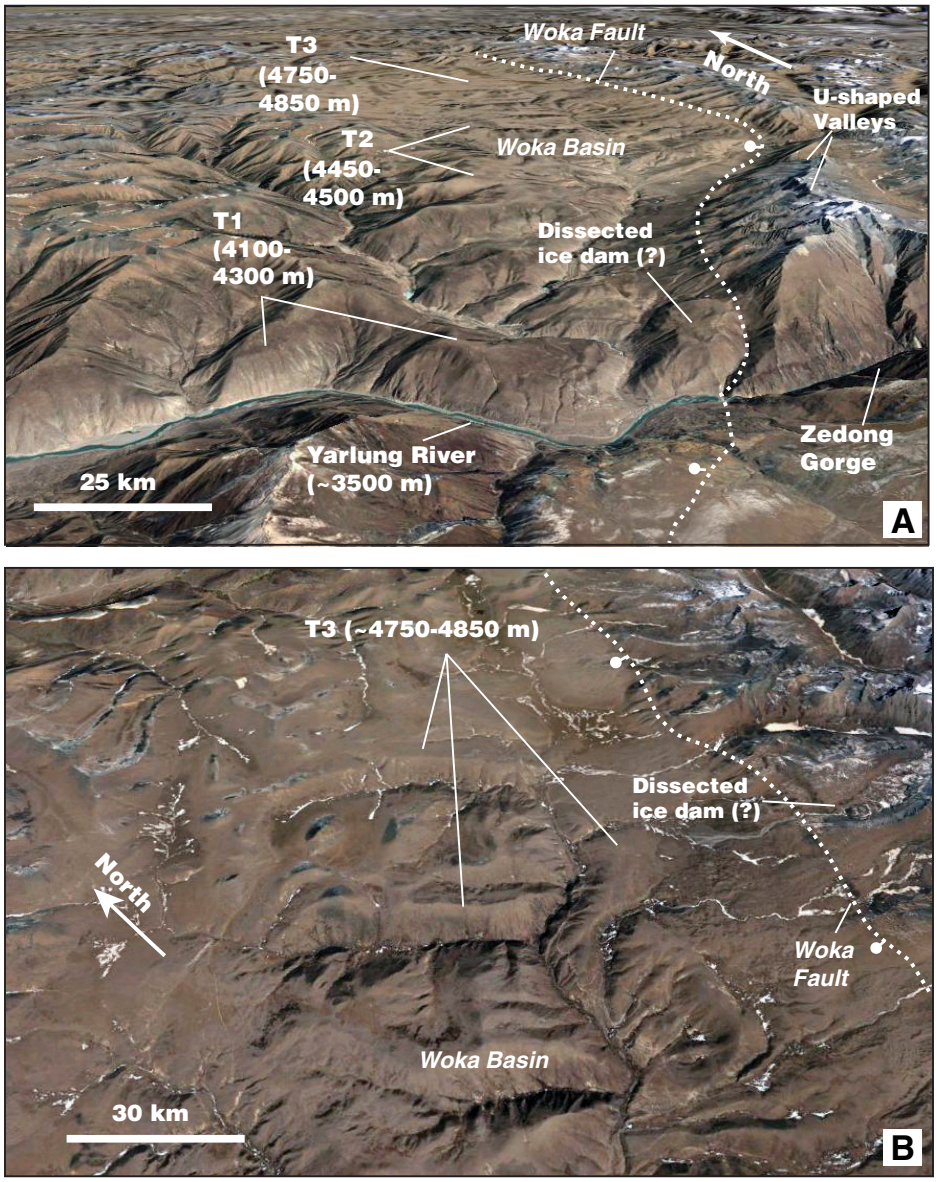

Figure 4. (A) Oblique Google Earth view of flat surfaces across the southern Woka rift basin north of the Zedong Gorge, Yarlung River. The surfaces are interpreted as treads of fluvial/lacustrine terraces. Note that their elevations correlate well with the elevations of the three sets of terraces south of the Zedong Gorge, Yarlung River. Also shown are the positions of hanging valleys along the glaciated ridge bounding the northern margin of the Woka basin. Location of the ice dam mapped by Korup et al. (2010) is also shown. (B) Oblique Google Earth view of the highest terrace surface in the northernmost part of the Woka rift basin.

are interlayered with diamicton composed of admixture of platy gravels of slate and schist, sandstone, and clay/siltstone (Fig. 6D). The diamicton is massive but locally displays thinly bedded clay and silt that are rich in dark organic material (Fig. 6D).

Although the cliff-forming upper member (Unit 3) (Fig. 6A) is similar in lithology and sedimentary structures to those in Unit 1, it differs from Unit 1 by its dominance in medium-grained (10–20 cm) and well layered gravels and laterally discontinuous sand lenses (2–5 m long) in contrast to sheet-like sand layers common in Unit 1. The unit is best exposed at the Luocun (~90 m thick), Sewu (~50 m thick), and the Siqunama–She Qu drainage divide sites (>50 m thick) at the deep-cut river banks (Figs. 3 and 5). At the Siqunama–She Qu divide along an east-west–trending trough, Unit 3 is exposed continuously over a distance of >7 km along the trough on both sides of the divide. Units 1 and 2 are missing east of the drainage divide, whereas Unit 3 rests directly on top of bedrock straths, which are composed of tilted Triassic strata. Sediments of Unit 3 is topped by a fill-terrace surface (T_3) and cut by several fill-cut terrace surfaces as represented by the formation of T_{3a} and T_{3b}.

Lithofacies

We conducted detailed lithofacies analysis to reconstruct the depositional settings of the valley-fill sequence. Lithofacies codes follow those of Miall (1977), Eyles et al. (1983), and Benn and Evans (2014). In addition, we adopted the mixed texture-lithofacies code of Gruszka (2001) (e.g., SG for gravelly sand, SF for silty sand, etc.) for describing more complex lithofacies.

Facies Sp. Medium-, coarse-grained, and gravelly sand associated with planar cross bedding occurs as both sand lenses (20–50 m thick and 2–4 m wide) and sand sheets (tens to ~100 m long) in Unit 1. However it is absent in Unit 2 and occurs only as sand lenses in Unit 3 (Figs. 5 and 6). This lithofacies is spatially associated with massive clast- and matrix-supported gravel beds in Units 1 and 3 (Figs. 5 and 6). The coarse-grained sand (1–2 cm) and fine-grained gravels (2–4 cm) are dominantly phyllite and slate, correlative with the Triassic strata of the Tethyan Himalayan Sequence exposed in the highlands surrounding the Sewu basin. Following Miall (1977) and Eyles et al. (1983), we interpret this lithofacies to have been deposited in transverse bars in a braided fluvial system.

Facies St. Medium-, coarse-grained, and locally gravelly sand associated with trough cross-bedding occurs as sand lenses (20–50 m thick and 2–4 m wide) in Units 1 and 3 within clast-supported massive to laminated gravel beds. However, this lithofacies is absent in Unit 2 (Figs. 5 and 6). Similar to the lithofacies *Sp*, the lithic fragments in coarse-grained sand (1–2 cm) and fine-grained gravels (2–4 cm) are dominantly phyllite and slate, correlative to the exposed Triassic strata of the Tethyan Himalayan Sequence in the study area (Fig. 1B). Following Miall (1977) and Eyles et al. (1983), we interpret this lithofacies to have been associated with the development of migrating dune fields on top of mid-channel bars in a braided fluvial system.

Facies Sl. Coarse-grained to very coarse-grained sand displaying horizontal to low-angle planar cross bedding occurs in both Units 1 and 3 (Figs. 5 and 6). It is commonly associated with channel fill in gravel beds. The filled channels are typically 20–50 cm high and 2–5 m wide. This lithofacies is interpreted to have been deposited in channels under lower flow regimes in a braided fluvial system (Miall, 1977; Eyles et al., 1983).

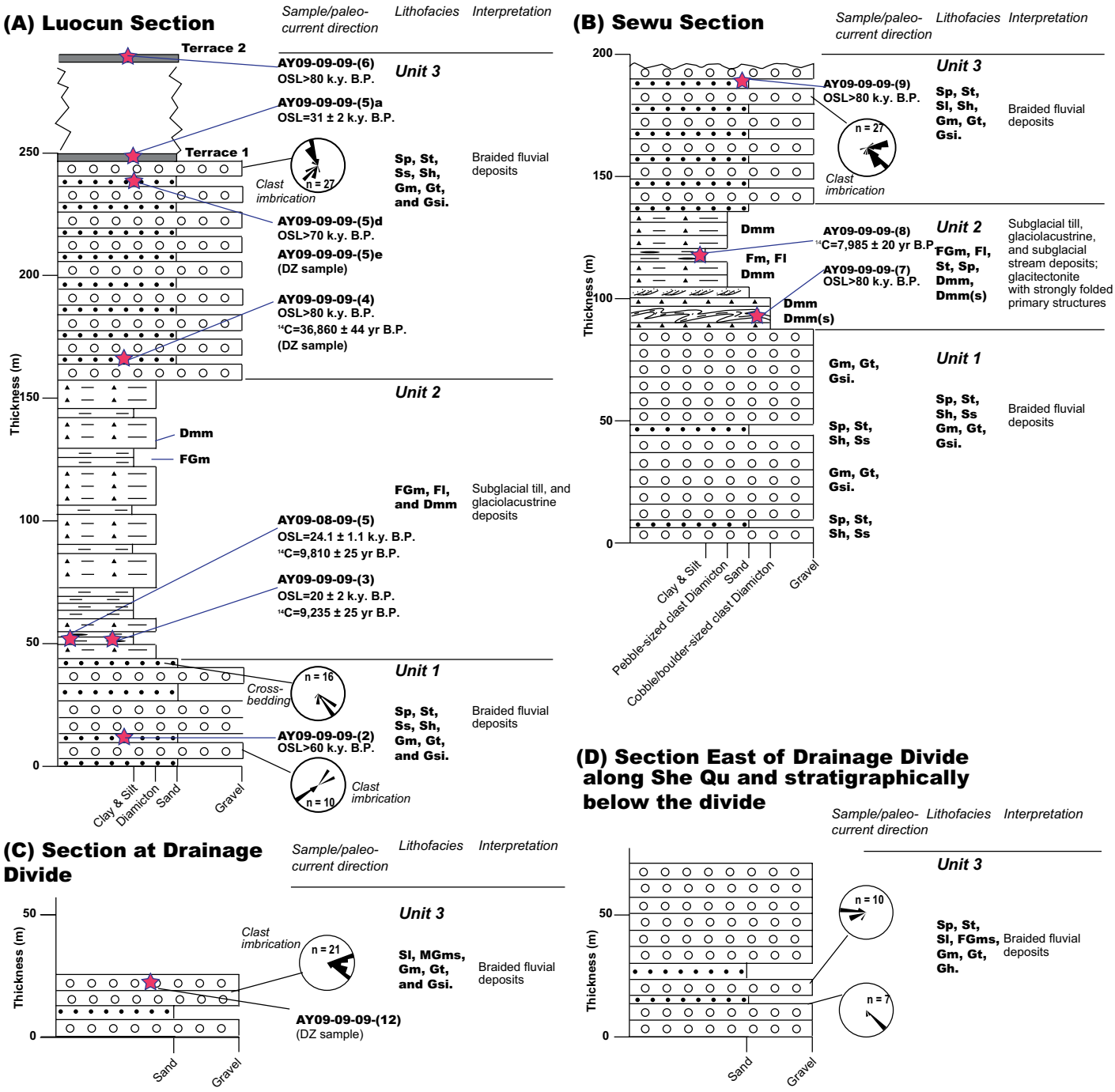

Figure 5. Stratigraphic division and associated lithofacies and paleocurrent directions of the Quaternary valley-fill sequence exposed in the study area. Locations of sections A to D are shown in Figure 3A. Stratigraphic positions of collected samples and the optically stimulated luminescence (OSL) and radiocarbon dating are also shown. Samples numbers with DZ represent stratigraphic positions of detrital-zircon samples used for U-Pb dating.

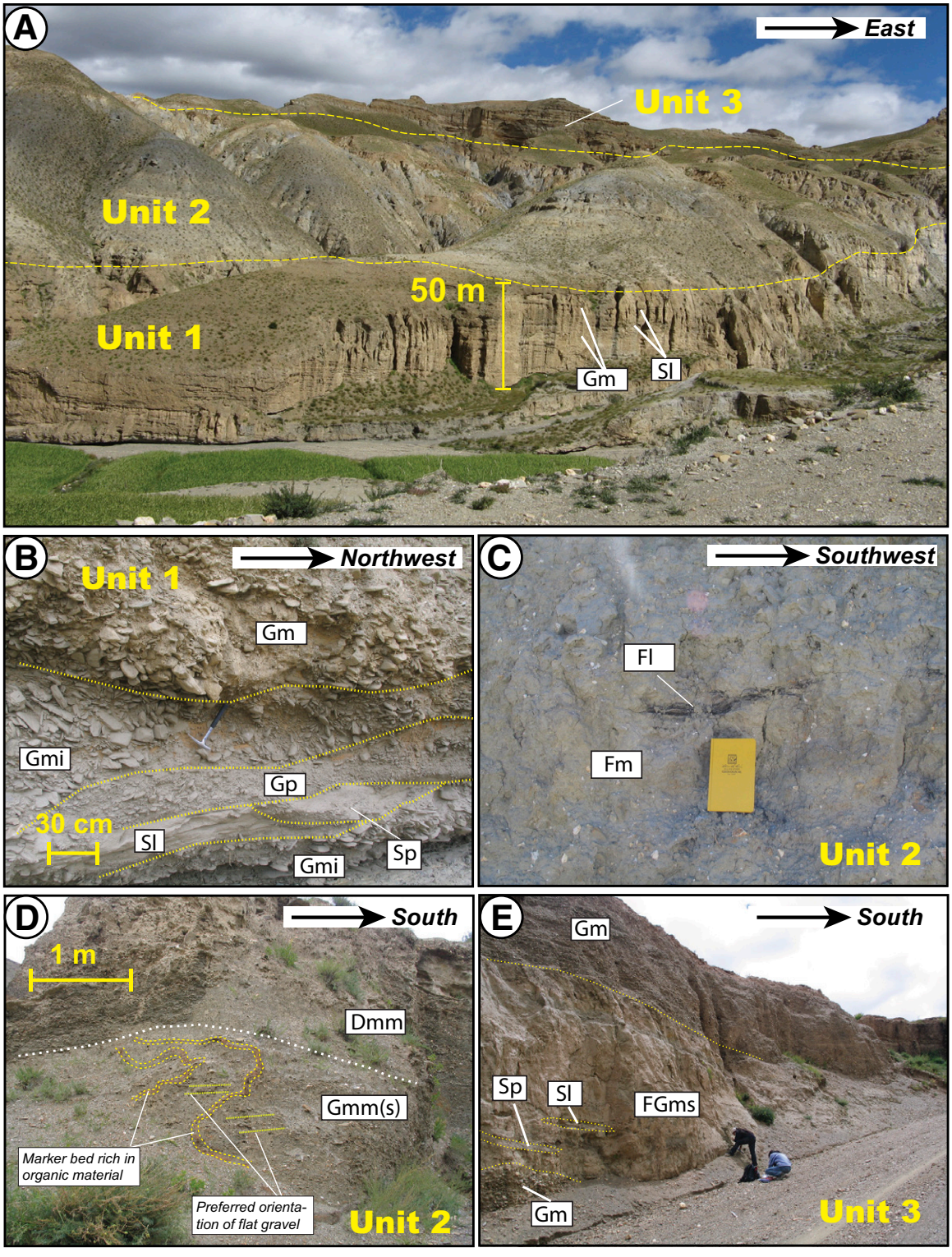

Figure 6. Field pictures of valley-fill sediments in the study area with the locations indicated in Figure 3A. (A) A view of three lithologic units east of Luocun. (B) Clast-supported boulder conglomerate interbedded with sand lenses in Unit 1. (C) Isolated peat layer in silty-matrix-supported glacial deposits (Unit 2). (D) Folded glacial deposits at the lowermost part of Unit 2. (E) Sand beds and overlying pebble conglomerate in the upper part of Unit 3. See text for abbreviations of lithofacies.

Facies Sh. Horizontally laminated coarse-grained to very coarse-grained sand occurs as channel fills in Units 1 and 3 (Figs. 5 and 6). In Unit 1, this lithofacies is commonly associated with the medium-bedded sheet-like sand that is interbedded with thickly bedded gravels (Fig. 6A). Deposition of this lithofacies is interpreted to have been associated with lower or upper flow regimes in a braided fluvial system on top of the intra-channel bars or within the stream channels (Miall, 1977; Eyles et al., 1983).

Facies Gm. This lithofacies defined by massive and crudely bedded gravels (Miall, 1977) is ~1–1.5 m thick and 15 to >50 m in lateral extent. Gravels are platy in shape, inherited from the bedding of the Triassic strata exposed in the study area and varying in shape from well-rounded to moderately rounded. The bedding is defined by the horizontal alignments of fine-grained (2–6 cm) to medium grained (6–15 cm) platy gravels associated with fining-upward grading (Fig. 6B). Gravels are both clast-supported and matrix-supported, where the matrix is dominated by medium- to coarse-grained sand. Matrix-supported lithofacies is best exposed in the lower section of Unit 1 in the Luocun section (Figs. 5A and 6B). The *Gm* lithofacies also displays erosive base and lateral variation in grain size. This lithofacies is interpreted to be longitudinal-bar or channel-lag deposits in a braided river system (Miall, 1977; Eyles et al., 1983). Alternatively, the lithofacies could have been deposited in an alluvial fan setting. However, the lack of inverse grading, mud matrix, boulder-size gravel, and angular clasts (Blair and McPherson, 1994; Weissmann et al., 2005) makes this interpretation unfavorable.

Facies Gt. Trough cross-bedded gravels are present in channels, bounded either by sand or gravels. The channels are 30–60 cm high and 1–3 m wide. We interpret this lithofacies as channel fill in a braided fluvial system (Miall, 1977; Eyles et al., 1983).

Facies Gmi. This facies is defined by clast-supported, massive, and imbricated gravels. It is well developed in Units 1 and 3. The imbricated pebbles are used to determine paleocurrent directions as shown in Figure 5. Imbricated pebbles are moderately to well-rounded. The Gmi lithofacies is 12–60 cm thick and a few meters to more than tens of meters thick in the bedding parallel direction. They also display a fining-upward grain-size distribution. This lithofacies is interpreted to be longitudinal-bar deposits.

Facies Gp. This facies is defined by planar cross-bedded gravels and is present in Units 1 and 2 (Figs. 5 and 6B). The thickness of the facies is 20–60 cm. This lithofacies is interpreted to be transverse- and/or linguoid-bar deposits, and the cross beds may have resulted from downstream migration of traverse bars and avalanches of the bar fronts in a braided fluvial system (Miall, 1977; Eyles et al., 1983).

Facies MGms and FGms. These facies are defined by matrix-supported medium- to fine-grained gravels with a normal grading. It is best exposed in the basal part of Unit 3 in the transitional zone from Unit 2 (Fig. 6E). This facies is interpreted to have originated from deposition of hyperconcentrated flows (Miall, 1985).

Facies Sp. This facies is characterized by medium- to very coarse-grained sand associated with planar cross bedding. Each lithofacies typically consists of 1–2 cross-bed sets that are 10–30 cm high and 50–150 cm long. This lithofacies is interpreted as transverse- or linguoid-bar deposits and the cross-beds are interpreted to have resulted from the frontal avalanches of the transverse- and linguoid bars (Miall, 1977).

Facies St. This lithofacies is rather rare and only present locally in Unit 1. The cross-beds are typically tens of centimeters long and 10–20 cm high and composed of medium- to coarse-grained sand. The lithofacies is interpreted to be transverse- and/or linguoid-bar deposits during the development and migration of sand dunes on top of the bars (Miall, 1977).

Facies Sh. This lithofacies consists of horizontally bedded medium- to very coarse-grained sand. Facies thickness varies from 30 cm to 120 cm, and its lateral extent ranges from a few meters to tens of meters. This lithofacies is interpreted to have been deposited through the migration of very low-amplitude sand waves on top of transverse/linguoid bars in shallow water of a braided fluvial system (Miall, 1977).

Facies Ss. The lithofacies is characterized by scour fillings of medium- to coarse-grained sand. The scours are typically tens of centimeters to 2 m wide and 15–40 cm high. The lithofacies is interpreted to have been created during an erosive stage followed by deposition of channel beds in a braided fluvial system (Miall, 1977).

Facies Dmm. This lithofacies is characterized by matrix-supported, massive diamictons. The clasts are angular and poorly sorted, with sizes ranging from a few cm to >30 cm. The orientations of the clasts are disorganized, whereas the matrix consists of silt and sand. This lithofacies occurs mostly in the upper part of Unit 2 and is interpreted to be subglacial till (Benn and Evans, 2014).

Facies Dmm(s). The lithofacies is similar to lithofacies Dmm except that (1) it contains thin layers of sand and silt that define bedding, and (2) the beds are isoclinally folded (see lithofacies *Gmm(s)* in Fig. 6D). This lithofacies is exposed in the Sewu area and lies below lithofacies *Dmm* (Figs. 5B and 6D). We interpret the lithofacies to have resulted either from debris-rich englacial folding (Goodsell et al., 2005) or shearing in the subglacial gliding zone (Evans et al., 2006; Benn and Evans, 2014).

Facies Fl. This facies consists of fine lamination of clay and silt that lack rhythmic sedimentation. This lithofacies occurs in the middle part of Unit 2 (Fig. 6C) and in places contains organic matter that may have been derived from decayed vegetation. The presence of dropstone in the lithofacies indicates that glaciers were calving into the lake at the time of clay deposition. We interpret this lithofacies to have been deposited in a glaciolacustrine setting (Gruszka, 2001).

Facies FGm. This facies is defined by gravelly silt and clay. The gravels are 2–5 cm, angular, and surrounded by clay and silt. Following Gruszka (2001), we interpret this lithofacies to have been deposited in a glaciolacustrine setting with ice rafts carrying and then delivering detritus to the lacustrine deposits. The lack of varves, typical of environments with annually varying physical processes in glacial lakes, means that the inferred lake may have been mostly subglacial, isolated from seasonal changes in temperature and thus sedimentation rate.

Clast Lithology, Paleocurrent Directions, Provenance, and Depositional Settings

The gravel lithology in Unit 1 varies across the study area. In the west, clasts are dominantly quartzite, slate, phyllite, and gneissic rocks correlative with lithology of the Yalaxiangbo dome (e.g., Zeng et al., 2011). In the north, clasts in Unit 1 are mainly sandstone and siltstone derived from Triassic strata in the Tethyan Himalayan Sequence. However, we did not observe any granitic clast that may have been derived from those in the Tethyan Himalayan Sequence (Aikman et al., 2008; Zeng et al., 2011) or the Gangdese batholith south and north of the Indus-Yarlung suture. The correlation between clast lithology and local sources indicates that sediments in Unit 1 were mainly derived from local highlands bounding the Siqunama drainage basin. Together with the lithofacies analysis, we interpret Unit 1 to have been deposited in a braided fluvial system; its paleocurrent directions are to the northeast and southwest in the lower section and to the southeast in the upper section at the Luocun section (Fig. 5A). The southeastward flow direction is particularly interesting, as it is in the opposite direction to the current flow of the Siqunama River along which Unit 1 strata are exposed.

Unit 2 was deposited during a phase of glacier advance, expressed by the deposition of subglacial tills, folded englacial and/or subglacial tills, and glaciolacustrine sediments. At Sewu, the vergence of the folded glacial deposits

indicates southward motion of the glacier flow. This is consistent with the glaciated morphology in the high mountains northeast of the study area (Fig. 2B).

The spatial variation of clast lithology of Unit 3 is similar to that of Unit 1 without any granitic clasts observed in the field. At Luocun in the west (Fig. 3) clasts are dominantly quartzite, correlative with metamorphic rocks of the Yalaxiangbo gneiss dome. At Sewu in the north, clasts are sandstone and siltstone that are correlative with Triassic strata exposed directly to the north in the glaciated highlands. Imbricated pebbles in lithofacies *Gmi* are used to determine paleocurrent directions during the deposition of Unit 3. At Luocun, well-rounded and imbricated platy pebbles indicate both northward and southwestward paleocurrent directions (Fig. 5A). At Sewu, pebble imbrication indicates a dominantly southward paleocurrent direction with a secondary eastward flow component (Fig. 5B). The paleocurrent directions at and near the drainage divide between the Siqunama River and She Qu vary vertically in Unit 3. At the highest stratigraphic level in the drainage divide area, the paleocurrent directions are east and southeast as determined by well-rounded and imbricated pebbles (Fig. 5C).

Directly east of the divide along She Qu, the middle part of Unit 3 displays eastward flowing paleocurrent indicators (i.e., well-rounded and imbricated pebbles) in the lower section and westward flowing paleocurrent indicators in the upper section (Fig. 5D). This observation suggests rapid flow-direction reversal, possibly as a result of a rapid shift in the drainage divide from west to east in the area.

Relationships between Uppermost Unit 3 and the Fill Terrace

The uppermost part of Unit 3 is well exposed at the drainage divide between the Siqunama River in the west and the She Qu in the east (Fig. 3). Because this part of Unit 3 has important implications for river diversion across the current Yarlung-Subansiri divide, we describe its relationship to the highest fluvial terrace with field photos (Fig. 7).

Figure 7A was taken at the drainage divide, which is situated at a broad and flat-bottomed trough, similar in morphology to a classic wind gap (e.g., Keller et al., 1998). The flat trough is 2–3 km wide and its trough walls, >100–150 m high, extend westward and eastward into the Siqunama River and She Qu (Figs. 7B and 7C). The valley walls of the Siqunama River and She Qu are narrow and steep at lower elevations, becoming open and gentle at higher elevations (Figs. 7B, 7C, and 7D). Unit 3 at the drainage divide (Fig. 7E) and the upper banks of the Siqunama River displays imbricated gravels (Fig. 7F) that require eastward and southeastward paleocurrent directions (Fig. 5C).

At one location, ~3 km east of the drainage divide along She Qu, Triassic strata are beveled to develop two levels of strath terraces (Figs. 3 and 7D). The higher terrace T_{3a}, overlain by 7–8 m strata of Unit 3, is ~50 m above the active stream channel, whereas the lower terrace T_{3b}, with no cover on the strath surface, is ~7–8 m above the active stream channel (Fig. 7D). The lowest strath surface lies some 150 m below the Siqunama–She Qu drainage divide. The strath surface may represent a paleo-river channel and its low elevation explains why Unit 3 sediments exposed along the upper Siqunama River banks below the current drainage divide display sedimentary structures suggesting an eastward "upslope" flowing direction, opposite to the current flow direction of the river along which the east-flowing strata are exposed.

AGE DETERMINATION OF QUATERNARY SEDIMENTS

Analytical Methods

We performed optically stimulated luminescence (OSL) dating of quartz grains and radiocarbon dating of peat and detrital charcoal grains to determine the depositional ages of Quaternary valley fill and terrace deposits. Below we describe the analytical methods used in this effort.

OSL dating. The effectiveness of the OSL dating technique depends on the completeness of bleaching of the dated quartz grains, which is controlled by the intensity and duration of daylight exposure before the dated grains were buried (e.g., Rhodes, 2011). The history and processes of quartz-grain generation are also important: grains recently eroded from bedrock are much more difficult to bleach than those experiencing multiple cycles of reworking at the surface (Rhodes, 2011). As our OSL samples were all collected from alluvial and glacial deposits from nearby mountains (mostly <5 km), it is highly likely that the OSL-dated quartz grains were incompletely bleached. Because of this, we regard all our OSL dates as representing the maximum deposition ages of the corresponding stratigraphic intervals where the samples were collected. We sampled only the finest components (usually medium- to fine-grained sand) from the generally coarse-grained alluvial and fluvial strata and silt from glacial deposits for OSL dating. All the OSL samples were collected as intact blocks and wrapped immediately in tin foil to limit exposure to sunlight. OSL age determination was performed at the Luminescence Dating Laboratory of Institute of Geology, China Earthquake Administration (CEA). Sensitivity-corrected multiple-aliquot regenerative-dose protocol (SMAR) was applied to eight samples while single-aliquot regenerative-dose protocol (SAR) was applied to the only remaining sample (Table 1) (Wang et al., 2005).

Radiocarbon dating. Prior to field sampling, the dated material might suffer from contamination from (1) younger carbon due to bioturbation or downward penetration of roots and younger humic acids, and (2) from older carbon residues including organic material, coal, or graphite eroded from local bedrock. Because of this, our target radiocarbon samples were pre-treated by removal of any visually obvious contamination at the W.M. Keck Carbon Cycle Accelerator Mass Spectrometer Laboratory in the University of California, Irvine. The target organic material was then sieved and treated with hot acid to dissolve older carbonates and with alkali solutions to remove younger humid acids that may coat the samples. After preheating, the target organic material was converted to graphite using the procedure described by Santos et al. (2004). Subsequently, the graphite was analyzed for $\Delta^{14}C$ using the Accelerator Mass Spectrometer of University of California at Irvine.

Although radiocarbon dating does not suffer from the problem of incomplete bleaching, interpreting the dates of charcoal grains also requires caution. This is because the charcoal grains could be detrital and recycled from older sedimentary strata. Due to the time lag between charcoal grain formation and charcoal-grain deposition, the radiocarbon ages of charcoal grains should only constrain the maximum depositional age of the corresponding stratigraphic sections where samples were collected. Peat materials incorporated by glacial tills may have formed in wet areas after glacier retreat (Benn and Evans, 2014), and thus, radiocarbon ages from peat materials also provide a maximum depositional age constraint but could be very close to the true age of glacial deposition.

Depositional Ages of Valley Fill

We collected valley-fill samples from the Luocun and Sewu sections where vertically continuous stratigraphic sections are exposed (Fig. 5) and their OSL dating results are summarized in Table 1 and radiocarbon dating results are summarized in Table 2. For direct comparison between OSL and radiocarbon dates, all OSL ages are quoted in the form of yr B.P. (i.e., before 1950), and the 61-year difference (i.e., the OSL analysis was conducted in 2010) in

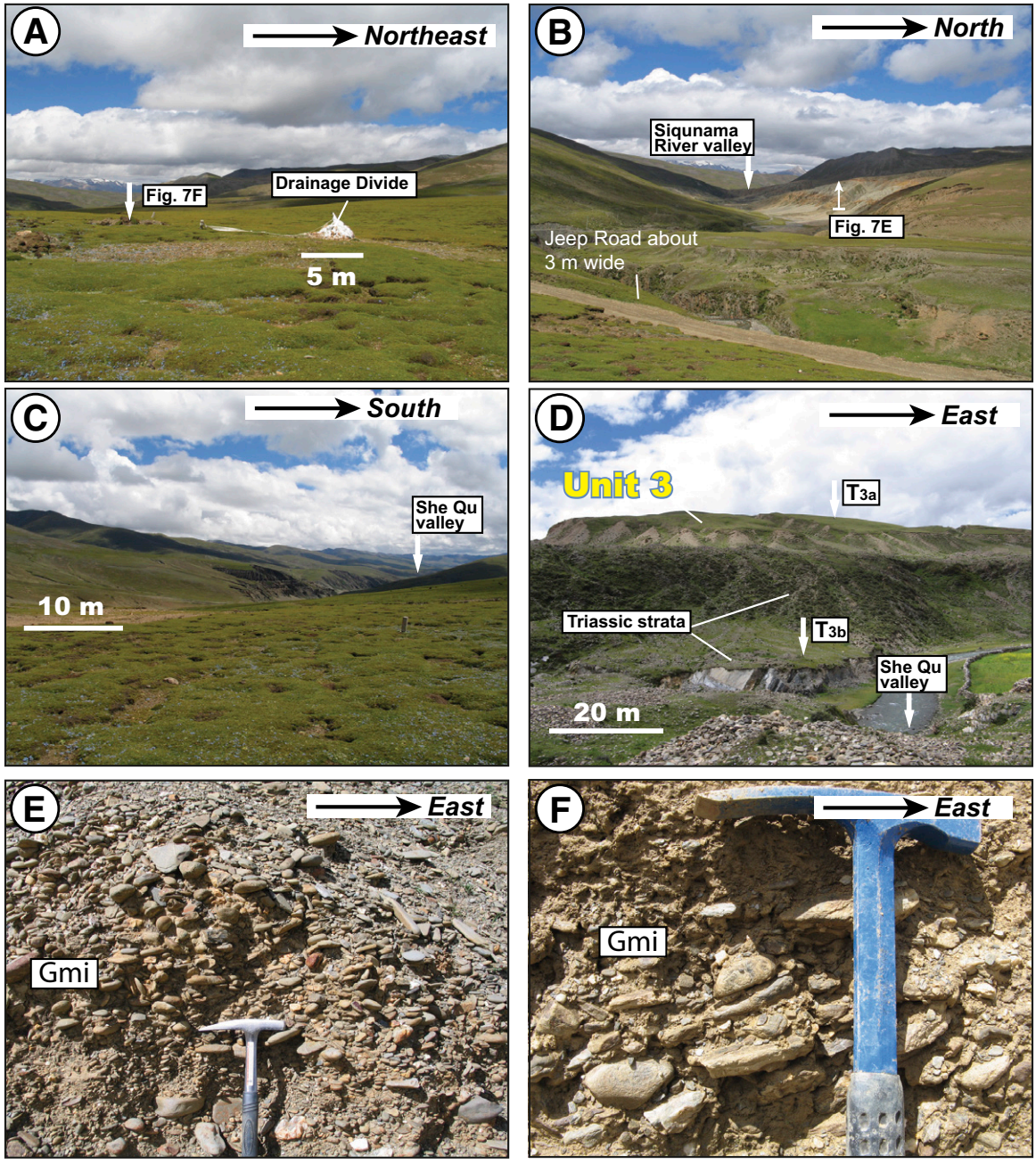

Figure 7. (A) Field picture of the drainage divide between the Siqunama River and She Qu. View toward the northwest. (B) Westward view of the Siqunama River valley from the drainage divide. Valley-fill sediments are exposed along the headwaters of the Siqunama River and can be traced ~3 km laterally west of the divide. (C) Eastward view of the She Qu valley from the drainage divide. (D) Northward view of two levels of strath terraces cutting tilted Triassic strata exposed ~3 km east of the drainage divide. The higher strath surface (T_{3a}) is ~50 m above the active stream with 10-m-thick valley-fill sediments of Unit 3, while the lower strath surface (T_{3b}) is ~7–8 m high with no alluvial sediments. (E) Well-rounded and imbricated pebbles in Unit 3 exposed west of the drainage divide. (F) Sub-rounded and imbricated pebbles in Unit 3 exposed at the Siqunama valley. The locations of the field pictures are shown in Figure 3A.

TABLE 1. OPTICALLY STIMULATED LUMINESCENCE DATING RESULTS FOR SAMPLES COLLECTED FROM THE VALLEY-FILL SEQUENCE AND FILL-TERRACE SEDIMENTS ALONG THE SIQUNAMA RIVER

Lab ID	Sample number	Note	Elevation (m)	Latitude (°N)	Longitude (°E)	Method	α counts (ks)	K (%)	Water (%)	Dose rate (Gy/ka)	De (Gy)	Age (k.y. B.P.)
(1) Luocun section												
09-402	AY09-09-09-(6)	Terrace T_2	4452	28.97136	92.15741	SMAR	11.98 ± 0.36	1.43	11	4.09 ± 0.18	Saturated	>80
09-400	AY09-09-09-(5)a	Terrace T_1	4242	28.95596	92.14434	SMAR	12.37 ± 0.38	1.58	10	4.33 ± 0.19	134 ± 10	31 ± 2
09-401	AY09-09-09-(5)d	Unit 3	4242	28.95596	92.14434	SMAR	11.89 ± 0.35	1.9	4	4.56 ± 0.20	>300 Gy	>70
09-399	AY09-09-09-(4)	Unit 3	4117	28.96273	92.14127	SMAR	16.16 ± 0.42	1.95	6	5.50 ± 0.24	Saturated	>80
09-398	AY09-09-09-(3)	Unit 2	4074	28.96079	92.13434	SMAR	11.65 ± 0.23	1.86	4	4.47 ± 0.20	91 ± 7	20 ± 2
09-396	AY09-08-09-(5)	Unit 2	4190	28.97872	92.14484	SMAR	11.27 ± 0.21	1.87	1	4.40 ± 0.20	106.1 ± 7.2	24.1 ± 1.7
09-397	AY09-09-09-(2)	Unit 1	4047	28.96141	92.13303	SAR	15.95 ± 0.25	1.81	2	5.31 ± 0.22	>300	>60
(2) Sewu section												
09-404	AY09-09-09-(9)	Unit 3	4386	28.97086	92.16801	SMAR	14.34 ± 0.33	2.06	5	5.24 ± 0.23	Saturated	>80
09-403	AY09-09-09-(7)	Unit 2	4267	28.95012	92.17509	SMAR	11.43 ± 0.35	1.9	4	4.47 ± 0.20	Saturated	>80

Note: SMAR—sensitivity-corrected multiple-aliquot regenerative-dose protocol for fine-grained quartz grains; SAR—single-aliquot regenerative-dose protocol for fine-grained quartz grains; K—content of radioactive potassium ^{40}K measured with the X fluorescence spectrum analysis; De—equivalent dose for the sample estimated in the lab.

TABLE 2. RADIOCARBON DATING RESULTS FOR SAMPLES COLLECTED FROM THE VALLEY-FILL SEQUENCE AND FILL-TERRACE SEDIMENTS ALONG THE SIQUNAMA RIVER

Lab ID	Sample number	Description	Elevation (m)	Latitude (°N)	Longitude (°E)	Graphite size		Fraction modern	$\Delta^{14}C$ (‰)	^{14}C age (yr B.P.)
						(mg C)	%C			
(1) Luocun section										
120718	**AY09-09-09-(4)**	**Unit 3, charcoal**	**4117**	**28.96273**	**92.14127**	0.079	0.49	0.0170 ± 0.0033	–983.1 ± 3.3	32,740 ± 1,560
120719	AY09-09-09-(4) rerun	Unit 3, charcoal (?)	4117	28.96273	92.14127	**0.369**	**0.55**	**0.0102 ± 0.0005**	**–989.9 ± 0.5**	**36,860 ± 440**
120716	**AY09-09-09-(3)**	**Unit 2, peat layer**	**4074**	**28.96079**	**92.13434**	0.208	3.58	0.3190 ± 0.0011	–683.4 ± 1.1	9180 ± 30
120717	AY09-09-09-(3) rerun	Unit 2, peat layer	4074	28.96079	92.13434	**0.529**	**4.34**	**0.3167 ± 0.0009**	**–685.7 ± 0.9**	**9235 ± 25**
120714	AY09-08-09-(5)	Unit 2, charcoal	4190	28.97872	92.14484	0.719	24.0	0.2948 ± 0.0008	–707.4 ± 0.8	9810 ± 25
(2) Sewu section										
120720	AY09-09-09-(8)	Unit 2, peat layer	4304	28.95786	92.17407	0.487	8.26	0.3702 ± 0.0009	–632.7 ± 0.9	7985 ± 20

Note: (1) Radiocarbon concentrations are given as fractions of the modern standard, $\Delta^{14}C$, and conventional radiocarbon age, following the conventions of Stuiver and Polach (1977). (2) Sample preparation backgrounds have been subtracted, based on measurements of ^{14}C-free. (3) All results have been corrected for isotopic fractionation according to the conventions of Stuiver and Polach (1977), with $\delta^{13}C$ values measured on prepared graphite using the accelerator mass spectrometer (AMS). These can differ from $\delta^{13}C$ of the original material, if fractionation occurred during sample graphitization or the AMS measurement, and are not shown. (4) Samples highlighted in bold had low amount of C in the first combustion. Second combustions were made when enough materials were available after the routine acid-base-acid (ABA) pretreatment protocol. Ages from the second combustions (with larger sample sizes) should be more reliable and are therefore interpreted as the final result. The discrepancies between the small and large reruns could be due to sample inhomogeneity.

the OSL and radiocarbon dates can be ignored due to ± 1 k.y. uncertainties of the OSL dates obtained in this study.

Unit 1. Sample AY09-09-09-(2) was collected from a fined-grained sand lens within a boulder conglomerate bed in Unit 1 at Luocun (Figs. 5A and 6). OSL dating yields a date of >60 k.y. B.P.

Unit 2. We dated four samples from Unit 2 (Figs. 5A and 6). Sample AY09-08-09-(5) was gray silt collected ~2.6 km northeast of Luocun. OSL dating of this sample yields an age of 24.1 ± 1.1 k.y. B.P., whereas radiocarbon dating of charcoal grains from the same sample yields an age of 9810 ± 25 yr B.P. The younger radiocarbon age from the same sample indicates that the dated quartz grains were incompletely bleached and the OSL dates should represent the maximum possible ages of deposition of the corresponding stratigraphic sections.

Sample AY09-09-09-(3) in Unit 2 was collected ~600 m east of and at a similar stratigraphic position to sample AY09-08-09-(5) (Fig. 3A). This sample yields an OSL date of 20 ± 2 k.y. B.P. Radiocarbon dating of peat material from the same sample yields a much younger age of 9235 ± 25 yr B.P. The much older OSL date than the radiocarbon date again indicates that the OSL dated quartz grains were incompletely bleached, most likely resulting from low sensitivity of quartz grains without any reworking at the surface, although they are interpreted to have been transported by a low-gradient braided river (Rhodes, 2011; Burgess et al., 2012). K-feldspar is generally believed to have higher OSL sensitivity with relatively rapid bleaching characteristics, and thus can be a better target mineral for OSL dating for these valley-fill sediments in future studies (e.g., Rhodes, 2011).

Sample AY09-09-09-(7) is silt collected at a site ~1 km north of Sewu from Unit 2. No organic material was obtained from this sample. OSL dating yields a date of >80 k.y. B.P., which should offer a maximum depositional age constraint due to incomplete bleaching under glacier-related environments.

Sample AY09-09-09-(8) was collected from a peat layer ~2 km north of Sewu. This sample yields a ^{14}C age of 7985 ± 20 yr B.P. Note that this sample is located stratigraphically above samples AY09-08-09-(5) and AY09-09-09-(3) that yield ^{14}C ages of 9810 ± 25 yr B.P. and 9235 ± 25 yr B.P., respectively. Thus, the younger

radiocarbon age of 7985 ± 20 yr B.P. from sample AY09-09-09-(8) is consistent with the stratigraphic relationship established in the field.

In summary, OSL dating yields maximum deposition ages of the dated sediments due to the effect of incomplete bleaching, which range from >20 k.y. B.P. to >80 k.y. B.P. for 50-m-thick Unit 2. This interpretation is consistent with the depositional settings of the dated material (glacial deposits) that most likely was derived from rapid erosion of bedrock and short-distance (<5 km) transport of sediments near the sample sites. The tight clustered radiocarbon ages of peat samples suggest their deposition at or slightly after 9.8–8.0 k.y. B.P. (Benn and Evans, 2014).

Unit 3. Three samples were collected from this unit (Figs. 5A and 6). Sample AY09-09-09-(4) was medium-grained sand within matrix-supported boulder conglomerate in the basal section of the unit. The sampling site is located ~1.5 km east of Luocun. The OSL date of the sample is >80 k.y. B.P., whereas radiocarbon dating of charcoal grains from the same sample yields a ^{14}C age of 36,869 ± 44 yr B.P. Sample AY09-09-09-(5)d is fine-grained sand in the uppermost part of Unit 3 and was collected from a site ~1.7 km southeast of Luocun (Fig. 3A). OSL dating yields date of >70 k.y. B.P. Sample AY09-09-09-(9) was collected from coarse-grained sand ~3.5 km north of Sewu (Fig. 3A). It yields an OSL date of >80 k.y. B.P.

In summary, all the OSL and radiocarbon dates obtained from Unit 3 are older than the radiocarbon ages of peats collected from the underlying glacial deposits in Unit 2. To reconcile this difference, we suggest that the OSL dates represent the maximum possible deposition ages due to incomplete bleaching of the dated quartz grains. As the dated charcoal grains may be detrital, we suggest the corresponding ^{14}C age of 36,869 ± 44 yr B.P. represents the formation rather than depositional age of the dated charcoal grains. This means that the radiocarbon age of 36,869 ± 44 yr B.P. should be treated as a maximum deposition age for the corresponding stratigraphic section of Unit 3.

Ages of Fill-Cut Terrace Deposits

Based on the cross-cutting relationships observed in the field, the fill-cut fluvial terraces in the study area must have been developed after the deposition of the valley-fill sequence. In order to determine the exact ages of fill-cut terrace development, we collected samples from lag deposits associated with terraces T_2 and T_1 using the OSL dating method. All dated samples were collected from the four stratigraphic sections shown in Figure 3A. The stratigraphic position of each dated sample is shown in Figure 5.

Terrace 2 Deposits. Sample AY09-09-09-(6) was collected from a fine-grained sand layer in a pebble conglomerate sequence at a road cut, whose base is not exposed. The sample was extracted ~30 cm below T_2 surface and yields an OSL date of >80 k.y. B.P. This date is much older than the age of the stratigraphically younger sediments obtained from radiocarbon dating of peat material as mentioned above. Because of this, we interpret the above OSL date to represent a maximum depositional age of the terrace lag deposits.

Terrace 1 deposits. Sample AY09-09-09-(5) a is fine-grained sand in the matrix of a pebble conglomerate layer. The sampling site located ~2 km east of Luocun lies ~80 cm below the T_1 tread surface. This sample yields an OSL date of 31 ± 2 k.y. B.P. This date is older than the depositional age of the stratigraphically younger sediments in Unit 2. Thus, we suggest that the dated quartz was incompletely bleached and the OSL date should represent a maximum depositional age of the dated sample.

The interpretation that the dated quartz from deposits of terraces T_1 and T_2 was incompletely bleached is consistent with the depositional setting of the two samples. Samples from both terrace deposits were collected from medium-grained sand as matrix in coarse-grained gravels. The lack of organic material from the terrace deposits prevented us from obtaining independent radiocarbon age estimates.

U-Pb DETRITAL-ZIRCON DATING

Evidence for paleocurrent directions from valley-fill sediments across the modern Yarlung-Subansiri drainage divide indicates that, under the assumption of unidirectional fluvial deposition, the presently north-flowing Siqunama River might have been temporarily incorporated into the south-flowing She Qu that is currently linked with the south-flowing Subansiri River. Because the Siqunama River is a tributary of the east-flowing Yarlung River, its capture by the She Qu and thus the Subansiri drainage system raises the question of whether this was a transient process with a local and small (less than a few km) shift or a regional and large (>20–30 km) shift of the Yarlung-Subansiri drainage divide. A large shift of the drainage divide during the aggradational event as established in this study would require a large portion, if not all of the discharge, of the east-flowing Yarlung River was captured during the drainage-divide shifting event.

In order to address this important question, we performed U-Pb dating of detrital zircon from four samples: two from the uppermost and basal parts of Unit 3 at Luocun and two from the uppermost section of Unit 3 at the Yarlung-Subansiri drainage divide. Sample locations are shown in Figure 2A and their stratigraphic positions are marked in the Luocun section shown in Figure 5A. The analytical data for U-Pb zircon dating can be found in GSA Data Repository.[1]

Analytical Method

Detrital-zircon dating using the U-Pb method was conducted at the Institute of Tibetan Plateau Research, Chinese Academy of Sciences in Beijing. The analysis was performed on an Agilent 7500a quadrupole–inductively coupled plasma–mass spectrometer (Q-ICP-MS) with a 193 nm excimer ArF laser ablation system. The first 15 seconds with laser off were used to collect the background values, and the following 40 seconds with laser on were employed to measure the peak intensities of the ablated material. Considering the size distribution of these detrital-zircon grains and signal stability, we adapted 25 μm ablation pits for all grains. The analytical procedure is similar to Xie et al. (2008) using Plesovice zircon and NIST SRM612 as standards. We employed cathodoluminescene (CL) imaging to investigate the internal structure of zircon grains and select target ablation sites with no fracture. For grains with the core-rim structure, we only analyzed the rim with its age recording the timing of the most recent thermal events. We dated ~100 grains per sample to detect age components that are >5% of the total at a 95% significance level (Dodson et al., 1988; Vermeesch, 2004). The complete analytical data can be found in the GSA Data Repository (see footnote 1).

Results of U-Pb Detrital-Zircon Dating and Comparison with Existing Data

Luocun section. Sample AY09-09-09-(4) collected from the base of Unit 3 (Figs. 3A and 6) yields 7.7% zircon grains with ages in the range of 210–290 Ma. The rest of the zircon ages are dominated by clusters at 510–570 Ma and ca. 1050 Ma, respectively (Fig. 8A). Sample AY09-09-09-(5)e collected from a sand lens at the top section of Unit 3, ~800 m southeast of sample AY09-09-09-(4) (Figs. 2A and 5), yields ~8% of the total dated grains in the range of 230–300 Ma with a main age peak at ca. 240 Ma (Fig. 8B). Two Early Cretaceous zircon ages at 108 Ma and 125 Ma are also obtained from

[1]GSA Data Repository Item 2016123, U-Pb detrital-zircon ages and the relevant analytical data, is available at www.geosociety.org/pubs/ft2016.htm, or on request from editing@geosociety.org.

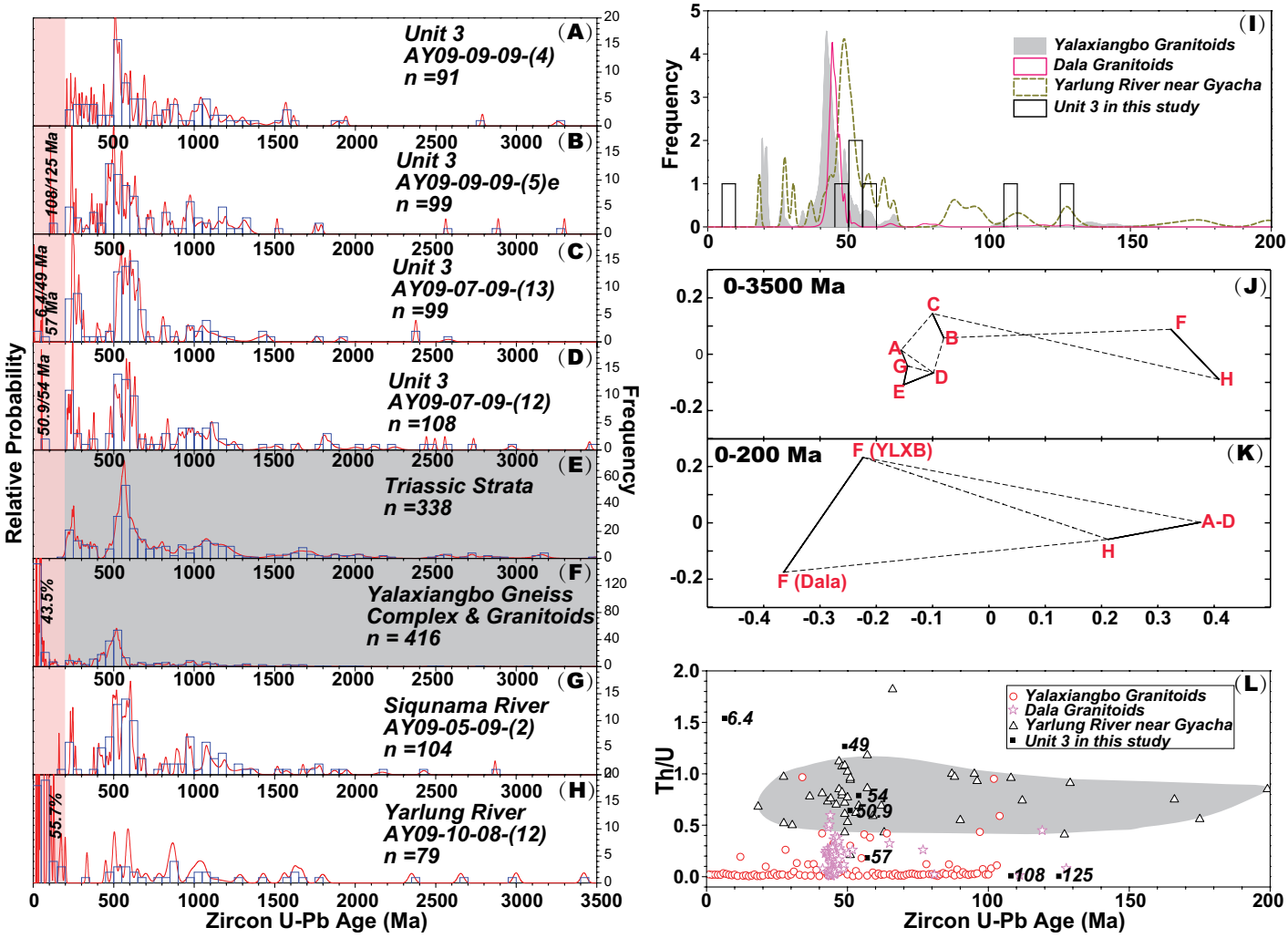

Figure 8. (A–D) Age spectra of detrital zircon in samples collected from Unit 3 along the Siqunama River valley. (E) Age spectrum of detrital zircon from Triassic strata of the Tethyan Himalayan Sequence after Aikman et al. (2008) and Webb et al. (2013). (F) U-Pb age spectra of detrital zircon from metasedimentary rocks of the Yalaxiangbo gneiss dome, zircon from Yalaxiangbo and Dala granitoids, and zircon from diabase dikes after Aikman et al. (2008, 2012a), Zeng et al. (2011), and Webb et al. (2013). (G) Detrital-zircon age spectrum of modern river sand from the Siqunama River obtained by Zhang et al. (2012). See sample location of AY09-05-09-(2) in Figure 1A. (H) Detrital-zircon age spectrum of modern river sand collected from the Yarlung River near Gyacha by Zhang et al. (2012). See sample location of AY09-10-08-(12) in Figure 1A. (I) Probability density plot in the range of 0–200 Ma for the U-Pb zircon from the Yalaxiangbo and Dala granitoids, and the Yarlung River sand, and frequency plot for detrital zircon from the valley-fill sediments of Unit 3. (J–K) are MDS (multidimensional scaling) plots for the U-Pb age data sets shown in A to H in the range of 0–3500 Ma and for the age data set shown in I in the range of 0–200 Ma. (L) Zircon Th/U ratio in the age range of 0–200 Ma for the Yalaxiangbo granitoids, Dala granitoids, the Yarlung River sand, and Unit 3.

this sample. An older-age cluster at 450–650 Ma accounts for 42.1% of the total dated grains, whereas the rest of the dated zircon grains have ages between 950 Ma and 1300 Ma (Fig. 8B).

Drainage-divide section. Sample AY09-07-09-(13) was collected from the upper part of Unit 3, which is ~3 km west of the Siqunama–She Qu drainage divide along the bank of the Siqunama River (Figs. 2A and 5). The dominant zircon ages cluster at 520–660 Ma and account for 47.5% of the total dated grains (Fig. 8C). A minor age group clusters at 960–1100 Ma. Additionally, 17.2% of the dated grains are at 240–300 Ma and show two age peaks at ca. 250 Ma and ca. 280 Ma, respectively. Three grains at 6 Ma, 49 Ma, and 57 Ma are also detected from this sample.

Sample AY09-07-09-(12) was collected from fine-grained sand in Unit 3 at the Siqunama–She Qu divide (Figs. 2A and 5). Zircon younger than 300 Ma accounts for 14.8% of the dated grains, which includes a dominant age cluster at 210–250 Ma and two grains dated at 51 Ma and 54 Ma (Fig. 8D). The age clustering at 480–650 Ma accounts for 34.3%. The rest of the dated grains have ages mostly at 900–1200 Ma (Fig. 8D).

Bedrock detrital-zircon ages. Detrital-zircon ages of Triassic strata surrounding our study area cluster at 230–270 Ma, 500–600 Ma, and 1000–1100 Ma (Fig. 8E), respectively (Aikman et al., 2008; Webb et al., 2013), whereas those from the Yalaxiangbo metamorphic rocks cluster at ca. 500–550 Ma (Fig. 8F) (Aikman et al., 2008, 2012a; Zeng et al., 2011; Webb et al., 2013). The 40–50 Ma Yalaxiangbo and Dala granitoids also yield minor Cretaceous zircon grains (Figs. 8F and 8I) (Aikman et al., 2008; Zeng et al., 2011).

Detrital-zircon ages of river sand. A sample from the Siqunama River near its confluence with the Yarlung River (i.e., AY09-05-09-(2) in Figs. 1 and 8G) yields the following age groups:

230–270 Ma, 500–600 Ma, and 1000–1100 Ma, respectively. Noticeably, the zircon age spectrum lacks the 40–45 Ma ages (Fig. 8G) despite the fact that the river drains both plutons. This result indicates that no 40–50 Ma zircon was delivered to the Yarlung River through fluvial transport. Thus, any 40–50 Ma zircon grain from the Yarlung River sand must have been derived from the Gangdese batholith in southern Tibet north of the river, which is the only source that deliver zircon of this age (Zhang et al., 2012). Based on the above inference, we quantified the Gangdese-derived detrital-zircon age component in the modern Yarlung River sand using the age spectrum of sample AY09-10-08-12 (Figs. 1B, 8H, and 8I) (Zhang et al., 2012). Zircon with ages of 40–70 Ma and 80–120 Ma from this sample accounts for >50% of the total dated grains.

Statistical analysis and correlation of Th/U ratios. We use the multi-dimensional scaling (MDS) method of Vermeesch (2013) to quantify the similarity and difference of the above mentioned U-Pb zircon age spectra. For the age range of 0–3500 Ma accounting for >90% of the total dated grains, the detrital-zircon age spectra from Unit 3 samples share the same age clusters at 230–270 Ma, 500–600 Ma, and 1000–1100 Ma as those from Triassic strata (Fig. 8J). However, Early Cretaceous to Eocene detrital-zircon ages detected from the Unit 3 samples are more similar to the age spectrum of the Yarlung River sand sample than those from the Yalaxiangbo and Dala granitoids (Fig. 8K). Furthermore, most of the Eocene zircon grains in Unit 3 samples have high Th/U ratios of >0.5, characteristic for Gangdese batholith zircon in the Yarlung River sand sample (Fig. 8L).

Comparison of zircon zoning morphology. The Early Cretaceous to Eocene zircon grains in Unit 3 samples display sub-angular geometry, simple internal textures, and rough grain edges. These features strongly resemble those dated from the Gangdese batholith in the Lhasa terrane north of the Indus-Yarlung suture zone and those detected in the modern Yarlung River sand near the Zedong Gorge (Zhang et al., 2012, and references therein) (Fig. 9). In contrast, the aforementioned textural features differ sharply from zircon grains of similar ages from the Yalaxiangbo gneiss complex (Zeng et al., 2011). Specifically, Early Cretaceous zircon grains from the Yalaxiangbo pluton have inherited ancient cores with Paleocene to Eocene rim ages; this feature is not observed from the Gangdese zircon grains (Fig. 9).

Summary of detrital-zircon age results. Based on the similarities in zircon ages, Th/U ratios, crystal shape, zoning morphology, and zoned age distribution, we suggest that the characteristic Cretaceous to Eocene detrital-zircon grains from the fluvial sequence of Unit 3 were sourced from the Gangdese batholith. That is, the Gangdese zircon was transported first by the Yarlung River, which in turn was linked to a fluvial system that transported Unit 3 sediments southward across our study area.

DISCUSSION

Major Findings from This Study

Our multidisciplinary study led to the following first-order findings:

(1) A major aggradational event occurred across the Yarlung-Subansiri drainage divide after 24–20 k.y. B.P. and continued until 9.8–8.0 k.y. B.P. (see the age summary in Fig. 5).

(2) The aggradational event was associated with a regional glacier advance event that is expressed by glacial deposits filling up the Woka-Yalaxiangbo rift basins north and south of the Zedong Gorge (see lithostratigraphy in Fig. 5).

(3) Three levels of major fluvial terraces are recognized both south (Fig. 3) and north (Fig. 4) of the Zedong Gorge with similar elevations. The highest terrace south of the Zedong Gorge slopes southward and lies above the current drainage divide between the Yarlung and Subansiri Rivers (Fig. 2C).

(4) Geomorphological evidence (i.e., U-shaped hanging valleys at the Zedong Gorge; see inset image in Fig. 2A) suggests that the Zedong Gorge was once jammed by glaciers and/or glacial deposits. Their similar elevations to the highest levels of fluvial terraces directly next to the gorge require a genetic linkage between the two geomorphological features, most likely through the expansion and shrinking of a large water body linked with the Yarlung River.

(5) Fluvial valley-fill deposits display complex flow directions (Fig. 5), which indicate rapid shifts in the Himalayan drainage divides in the study area. Sedimentary structures in the uppermost part of the valley-fill sequence indicate the occurrence of a transient southward flow across the modern Himalayan divide between the east-flowing Yarlung River and south-flowing Subansiri River.

(6) U-Pb detrital-zircon dating of samples from the uppermost valley-fill sequence reveals a minor fraction (0%–3%) of Cretaceous to Eocene ages; their similarities in age (Figs. 8A–8K), Th/U ratios (Fig. 8L), crystal shape (Fig. 9), zoning morphology (Fig. 9), and zoned age distribution (Fig. 9) to those from the Gangdese batholith suggest that the fluvial system transporting Unit 3 sediments was linked with the Yarlung River system.

Based on the observations made in this study, we propose the following scenario for the deposition history of the valley-fill sequence examined in this study. Unit 1 strata were deposited in a south-flowing braided river system, which could be induced by an ice dam either along the Siqunama River or the Yarlung River (Fig. 10A) (see detailed discussion below). This river was internally drained during Unit 1 deposition, with the fluvial sediments accumulated in areas south of the modern Siqunama–She Qu drainage divide. This interpretation requires the presence of lacustrine facies deposits, which are not exposed in the study area. We suggest that the inferred lacustrine facies strata coeval with deposition of Unit 1 was buried by the younger valley-fill sediments of Units 2 and 3.

The braided fluvial setting during deposition of Unit 1 was replaced by glacial deposition during the period of high snow accumulation in the highlands surrounding the Siqunama basin (Fig. 10B). The advancing glaciers may have terminated at a lake that received calved icebergs from the banks of the lake. A decrease in precipitation across southeast Tibet and the eastern Himalaya may have caused glacier retreat. However, the valley-fill sequence associated with glacial advance had raised the channels high enough to allow the development of a south-flowing braided river system during the deposition of the lowermost part of Unit 3 (Fig. 10C). The flow direction became westward during deposition of the middle part of Unit 3 (Fig. 10D), while the flow direction became southward during the deposition of the topmost part of Unit 3. At this time, we infer that a through-going river was developed across the modern divide between the Yarlung and Subansiri Rivers (Fig. 10E). This event was followed by fluvial incision of the loosely valley-fill sediments, leading to the establishment of the modern Siqunama River–She Qu divide and formation of a series of fill-cut terraces along the Siqunama River and She Qu (Fig. 10F).

Late Quaternary Himalayan Climate History and Glaciation

The Himalayan climate system is controlled by the mid-latitude westerlies and the south Asian summer monsoon (e.g., Benn and Owen, 1998; Yao et al., 2012). The westerlies affect alpine glaciation in the westernmost Himalaya, whereas the south Asian monsoon dictates precipitation to the rest of the Himalaya (Benn and Owen, 2002; Owen and Benn, 2005; Owen et al., 2008; Owen, 2009; Yao et al., 2012). Quaternary history of the south Asian monsoon is recorded in sediments of the Arabian Sea and the Bay of Bengal (Gupta et al., 2003; Kudrass

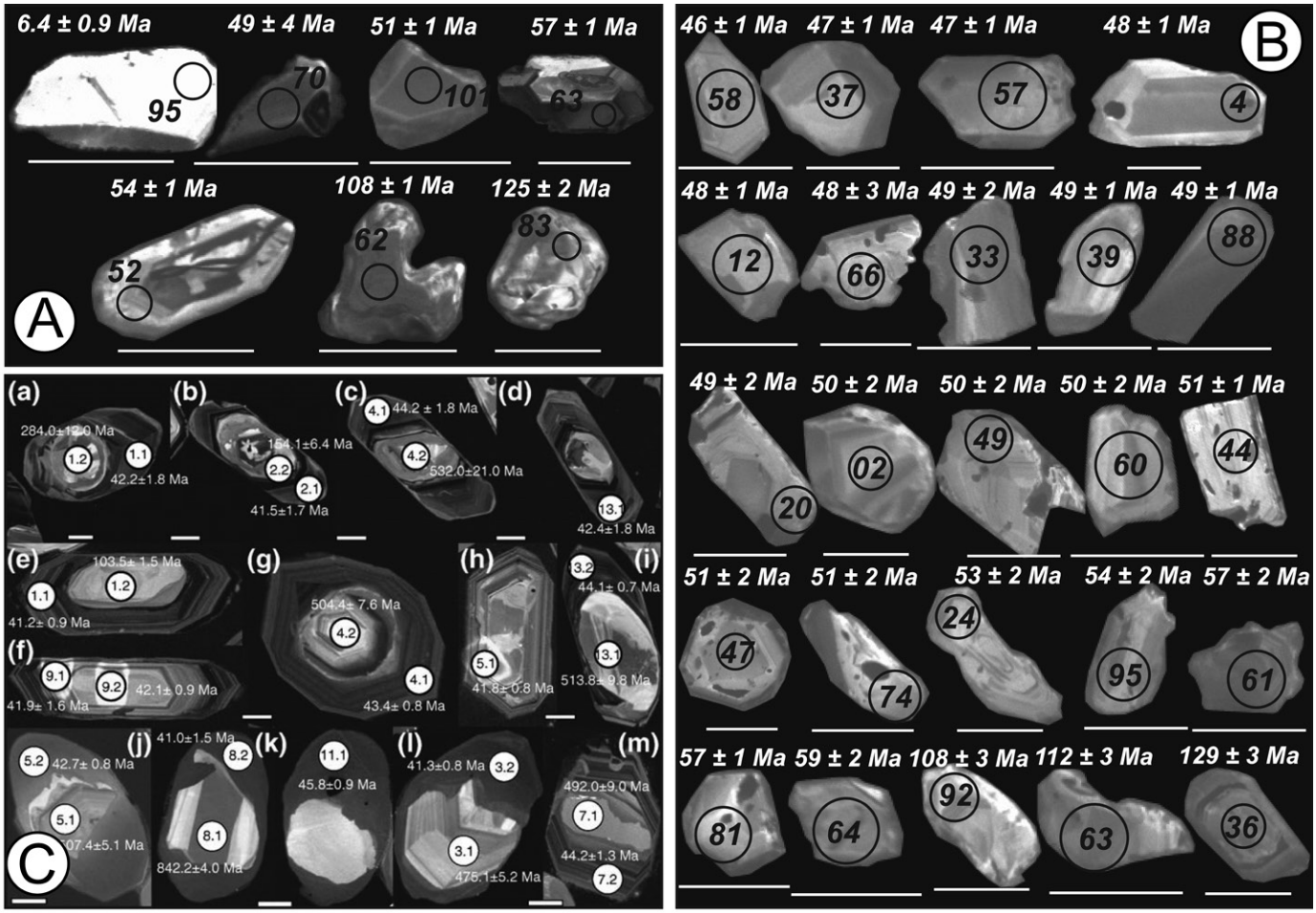

Ⓐ Zircon grains of 0-200 Ma age from the valley-fill sediments along the Siqunama-She Qu river valley; scale bar for all zircon grains: 100 μm

Ⓑ Zircon grains of 0-200 Ma age from river sand of the Yarlung River near Gyacha (Zhang et al., 2012); scale bar for all zircon grains: 100 μm

Ⓒ Zircon grains of 0-200 Ma age from the Yalaxiangbo gneiss complex and related granitoids (Zeng et al., 2011); scale bar for all zircon grains: 25 μm

Figure 9. (A) Cathodoluminescence (CL) images of zircon grains with ages of <200 Ma from samples AY09-09-09-(5)e (spots 62 and 83), AY09-07-09-(13) (spots 95, 70 and 63) and AY09-07-09-(12) (spots 101 and 52) collected from the uppermost part of Unit 3. (B) CL images of zircon grains from modern river sand of the Yarlung River collected near Gyacha directly east of the Zedong Gorge obtained by Zhang et al. (2012) (i.e., AY09-10-08-12 with its location shown in Fig. 1A). Note the similarities of zircon zoning and shape for those dated from samples collected from the Quaternary valley-fill sequence in the study area with these Gangdese-derived detrital-zircon grains. (C) CL images of zircon grains from the Yalaxiangbo gneiss complex and Eocene granitoids after Zeng et al. (2011). Note that the zircon grains from the Yalaxiangbo dome have highly irregular shape and lack well-defined zonation.

et al., 2001; Chauhan, 2003; Goodbred and Kuehl, 2000), cave deposits from the western Himalaya (Burns et al., 1998; Neff et al., 2001; Fleitmann et al., 2003; Sinha et al., 2005), peat deposits from the Tibetan Plateau (Hong et al., 2003), ice cores from western Tibet (Thompson et al., 1997), and lacustrine sediments from both the Gangetic floodplains and the Tibetan Plateau (Sharma et al., 2004; Wang et al., 2002; Liu et al., 2008). Together, they indicate (1) monsoon weakening during the Last Glacial Maximum (LGM) (24–19 k.y. B.P.), resulting in a cold and dry period lasting until ca. 15 k.y. B.P., (2) monsoon intensification at 15–11 k.y. B.P., (3) millennial-scale oscillation of weak and strong phases of the summer monsoon at 10.4–5.5 k.y. B.P., and (4) successive shifts toward drier conditions punctuated by intensified glaciation at 5.0–4.3 k.y. B.P. and ca. 2.0 k.y. B.P. (Anderson et al., 2002; Gupta et al., 2003; Chauhan, 2003). Our recorded glacier advance event at 9.8–8.0 k.y. B.P. was overlapping in time with the millennial-scale oscillation of weak and strong phases of the South Asia summer monsoon at 10.4–5.5 k.y. (Owen et al., 2008; Owen, 2009).

One of the consequences of glacier advance was the formation of ice dams composed of glaciers and glacial deposits across the Yarlung River drainage basin in the eastern Himalaya (Korup and Montgomery, 2008; Korup et al., 2010). The ice dams typically formed in narrow gorges where active normal faults cut across (Zhang, 2001; Korup et al., 2010). An early Holocene glacial damming event was documented by Montgomery et al. (2004) at the Yarlung Gorge,

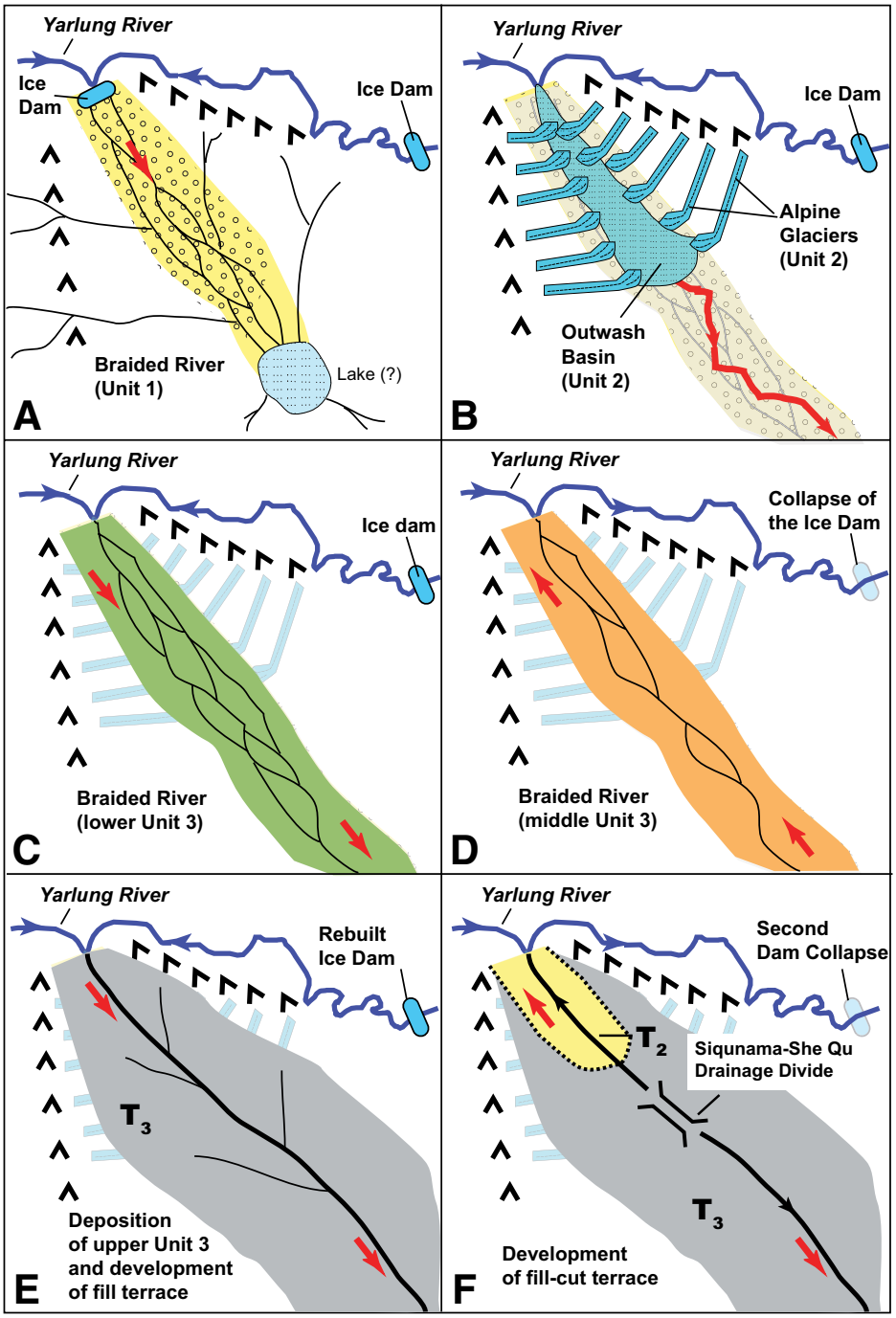

Figure 10. Depositional history and geomorphologic evolution of the Siqunama drainage basin. See text for details.

where the highest lacustrine terraces at ~680 m above the current river level were dated at ca. 8.2–9.4 k.y. B.P. This age is coeval with the glacier advance event documented in our study area at 8.0–9.8 k.y. B.P., suggesting that the ice dam formation was widespread along the Yarlung River. Recent work of Liu et al. (2015) suggests that the onset of ice damming may have started as early as 41 k.y. B.P. in the eastern Himalayan syntaxis area, but the context of this older event is poorly understood.

Local versus Regional Ice Dam Models

Glacial lakes are common features in the Himalaya that are formed by dams created by flowing alpine glacier or moraine deposits (e.g., Richardson and Reynolds, 2000). Ice-dammed glacial lakes are commonly associated with glacier advance events when the accumulation rate of snow is greater than the ablation rate of the glacier (Richardson and Reynolds, 2000; Montgomery et al., 2004). In contrast, moraine-dammed glacial lakes generally result from glacier retreat (e.g., Richardson and Reynolds, 2000) (Fig. 11). The ice and moraine dams may only partially block a flowing river, with the outflow either percolating below the dam via a tunnel or by breaching the dam margins (Richardson and Reynolds, 2000). To place our inferred geological processes into an actualistic geologic context, we envision that glacier advance during a period of high precipitation led to the aggradation and river diversion event as summarized in Figure 10. We present two end-member ice-dam models: a local dam that blocked the outlet of the Siqunama River, and a regional dam on the Yarlung River (Fig. 12). We hope that the two models will better guide the future research on the important problem of Himalayan drainage evolution.

The consequence of a local damming at the Siqunama River (i.e., jamming at the Qusong Gorge) is illustrated by the longitudinal-profile relationships among the Yarlung River, Siqunama River, and She Qu (Fig. 12A). The water levels of an internally drained lake at different stages of glacial damming at the Siqunama River are also shown in Figure 12A, corresponding to the scenarios shown in Figures 12D and 12E. The local damming scenario requires the thickness of the valley-fill sequence to be at least 800 m in order to generate a south-flowing fluvial sequence overlying the current Yarlung-Subansiri drainage divide (Fig. 12A). We envision that the drainage-system geometry was similar to that today prior to 24–20 k.y. B.P.: the Siqunama River flowed northward into the Yarlung River (Fig. 12C). As a result of local damming at the Qusong Gorge along the Siqunama River, an internally drained Sewu basin was fed by the south-flowing lower reach and the north-flowing upper reach of the Siqunama River (Fig. 12D). This scenario is consistent with the inferred depositional setting and paleocurrent directions as shown in Figure 10. The gradual increase in the height of the local dam at the Siqunama River led to the overspill of the Sewu basin across the Yarlung-Subansiri drainage divide (Fig. 12E).

In contrast to the local damming scenario, the regional damming scenario involves a glacial dam on the Yarlung River and formation of a large lake fed by the Yarlung River west of the Zedong Gorge (Figs. 12D′, 12E′, 12F, and 13). We suggest that rapid advance of alpine glaciers originating from the high peaks that intersect the

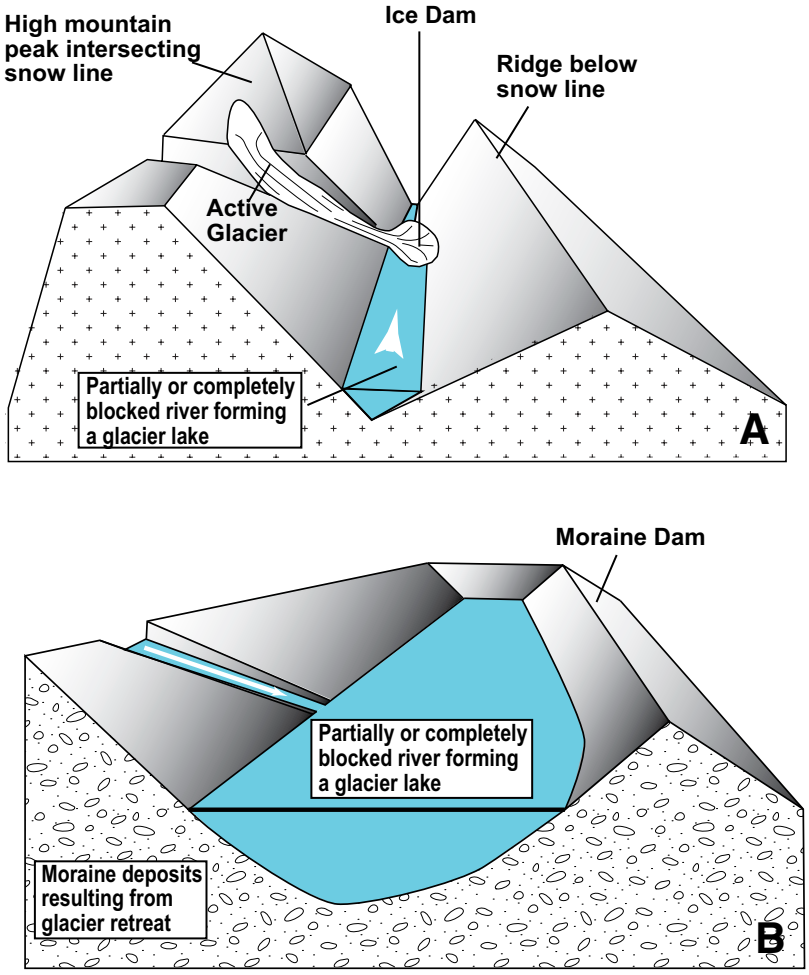

Figure 11. Schematic diagrams showing the formation of a glacial lake as a result (A) damming by a flowing glacier during glacier advance, and (B) damming by moraine deposits after glacier retreat.

local snow lines and bound the Zedong Gorge led to the formation U-shaped hanging valleys along the gorge (Fig. 13A). Advancing glaciers had also resulted in the formation of an ice dam that blocked the outflow of the Yarlung River and trapped sediments in a large ice-dammed lake covering both the Siqunama and Woka basins west of the Zedong Gorge (Figs. 13B and 13C). The sedimentation rate in the ice-dammed lake must have been very high at the time of the ice-dam formation, as the detritus was likely to have been largely derived from rapidly eroded glaciated terrains across the Yarlung River basin at the time when the regional climate was punctuated by the intensified South Asia summer monsoon with precipitation (e.g., Owen et al., 2008; Owen, 2009). It is important to note the role of tectonics in the controlling the ice dam formation. That is, it is because the extension along the Woka-Yalaxiangbo fault zone created a local high topography (i.e., rift shoulder) extending upward and intersecting the snow line. This special condition allows glaciers to form at high altitudes, while the Yarlung River below the snow line is still capable of flowing through the narrow Zedong Gorge. However, when the accumulation rate of snow for the glaciers originating from the high rift-shoulder topography is greater than the glacier ablation rate, the mass and length of the glaciers extend downward and can eventually intersect and block the Yarlung River at the Zedong Gorge as shown in Figure 13C. In contrast, the ice dam is removed when the accumulating rate of snow is less than the ablation rate of the glaciers sourcing from the high rift-shoulder topography (Fig. 13D). A consequence of ice damming at the Zedong Gorge and sediment aggradation in the large lake west of the gorge that covers both the Woka and Sewu basins (Fig. 12E′) is a change in the regional topography. Specifically, when the aggradation and/or lake level rose above the drainage divide between the Yarlung and Subansiri Rivers, the lake water fed by the upper stream of the Yarlung River would have spilled over the divide, which explains the deposition of a southward flowing fluvial sequence in the upper streams of the Siqunama River and She Qu observed in this study. Regardless of local or regional damming, the removal of the glacier dam(s) as a result of a drastically decreased precipitation rate in the region caused fluvial incision and the formation of the three levels of major fill-cut terraces in the Woka and Sewu basins.

In the regional damming hypothesis, the top of the ice dam must be ~1.3 km above the current river. This inference is consistent with the elevation of the U-shaped hanging valleys currently exposed along the two sides of the rift-controlled steep Zedong Gorge walls. Using the height of U-shaped valleys to infer the elevation of a past glacier surface is well-established and has been applied to the geomorphological studies of the iconic Yosemite Valley (e.g., Matthes, 1972). In contrast to the formation of the Yosemite Valley where glaciers were derived from line sources feeding the main valley, the Zedong Gorge is bounded by rift-induced point sources that allow the long course of the Yarlung River course to be jammed locally. Also note that the relief between the elevation of the U-shaped valleys and current Yarlung River channel at the Zedong Gorge only measures the maximum height of the ice dam, as the base of the dam could have been composed of aggradated sediments.

The regional damming scenario implies a drastically enlarged upstream drainage basin of the Subansiri River, which would have caused transient but rapid erosion in the lower reach of the Subansiri River. Enlargement of the Subansiri drainage basin also requires the existence of a wide stream channel compatible with the size of the drainage area. This expectation is consistent with the channel width of >2 km as required by the distribution of T_3 sediments at the Siqunama–She Qu divide (Fig. 3A). Considering the great difference in drainage area between the current Siqunama River and a linked Yarlung-Subansiri River required by the regional damming scenario, the effect of increasing precipitation on channel widening can be neglected (Snyder et al. 2000; Montgomery and Gran, 2001; Whittaker et al., 2007; Attal et al., 2008). Thus, we suggest that the formation of a wide south-flowing channel at the Siqunama–She Qu divide region was caused by capturing of the upper stream of the Yarlung River by the south-flowing Subansiri River. In addition, the regional damming model explains the presence of Cretaceous-Eocene detrital zircon of the Gangdese affinity in the valley-fill sequence (Fig. 8).

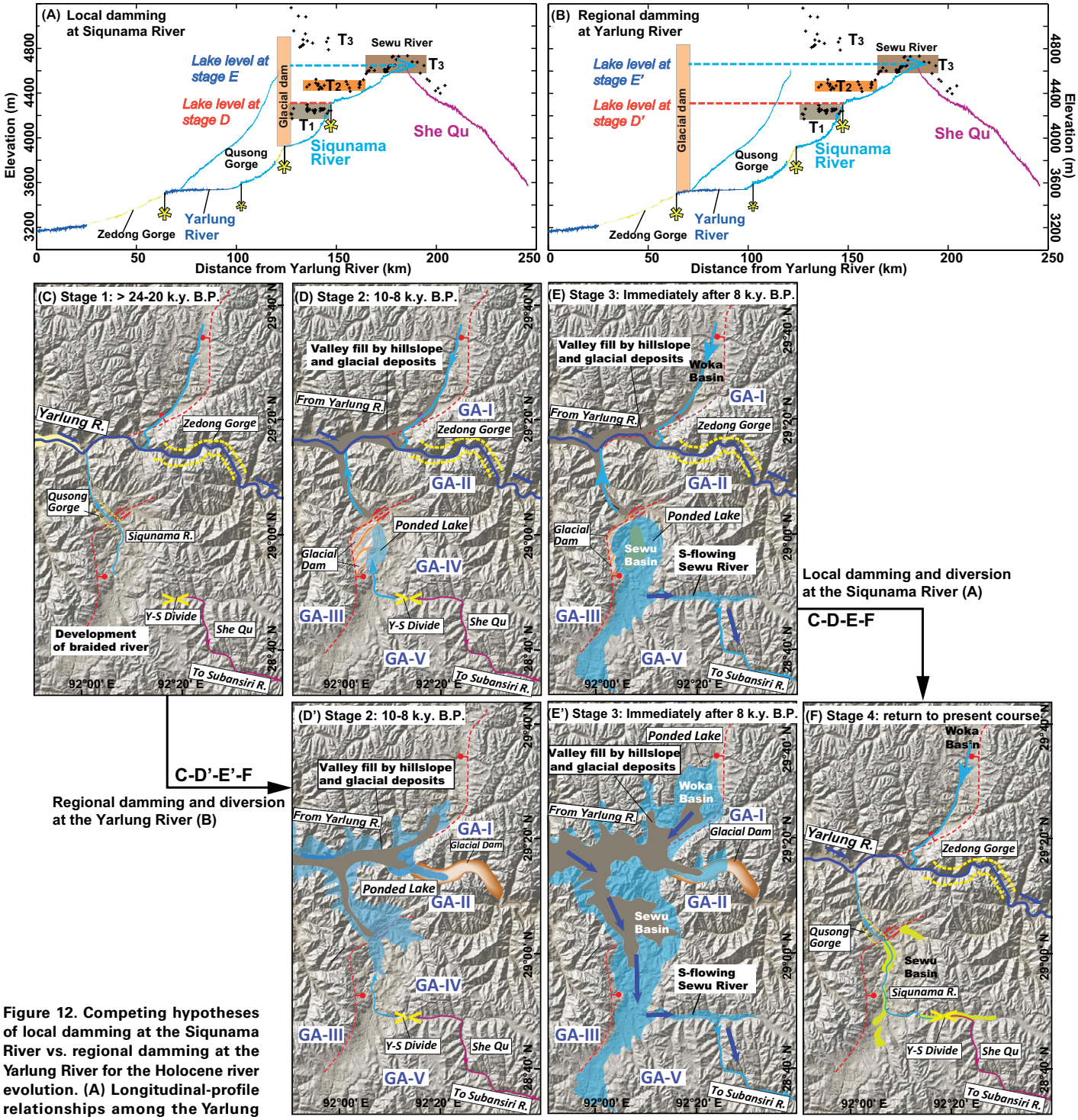

Figure 12. Competing hypotheses of local damming at the Siqunama River vs. regional damming at the Yarlung River for the Holocene river evolution. (A) Longitudinal-profile relationships among the Yarlung River, Siqunama River, and She Qu and the lake levels during different stages of glacial damming at the Siqunama River. Also shown are major knickzones and elevation distribution of fluvial terraces along the Siqunama River. (B) Longitudinal-profile relationships among the Yarlung River, Siqunama River, and She Qu and the lake levels during different stages of glacial damming at the Yarlung River. Also shown are major knickzones and elevation distribution of fluvial terraces along the Siqunama River. (C) Prior to 24–20 k.y. B.P., the drainage system geometry is inferred to have been similar to that today, with the Siqunama River flowing northward into the Yarlung River. (D) As a result of local damming, an internally drained basin, here referred to as the Sewu basin, was fed by the south-flowing lower reach and north-flowing upper reach of the Siqunama River. (E) The gradual increase in the height of the local dam led to the overspill of the Sewu basin across the Yarlung-Subansiri drainage divide. The through-going river is referred here as the Sewu River. (D') In contrast to (D), the regional damming scenario requires the formation of a large lake west of the Zedong Gorge as shown. At this time, alpine glaciers filled up the Zedong Gorge, which led to ponding at the interconnected Woka and Sewu basins. (E') The gradual increase in the height of the regional dam at the Zedong Gorge of the Yarlung River led to the spill over the Sewu basin across the Yarlung-Subansiri drainage divide. (F) The removal of the local or regional glacier dam led to fluvial incision into the valley fill created during the damming event. The incision eventually created the modern drainage pattern.

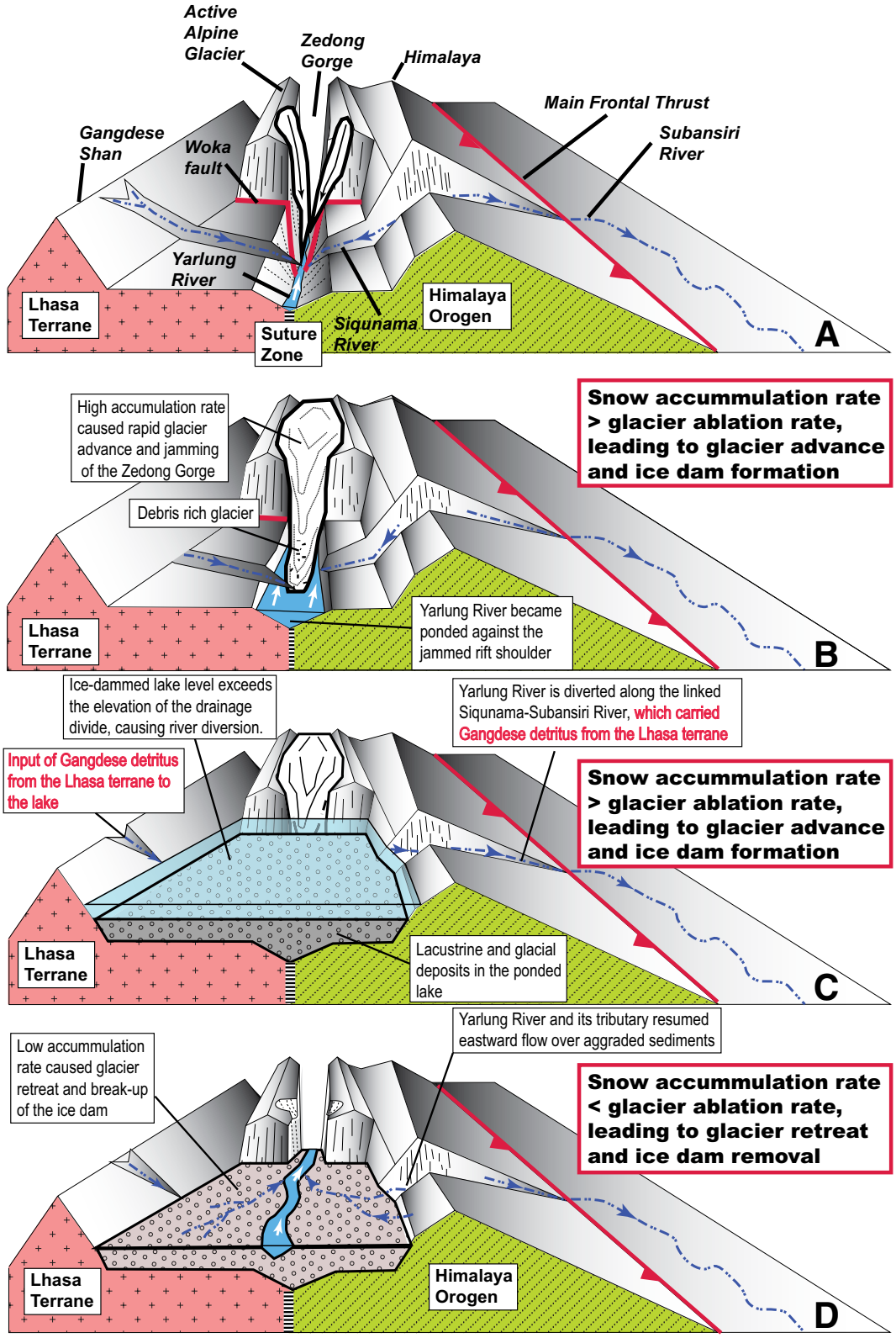

Figure 13. Block diagrams showing the evolution of the Yarlung and Subansiri Rivers during the formation and removal of an ice dam at the Zedong Gorge. Note that the diagram illustrates how the Gangdese detritus of the Lhasa terrane was transported across the Himalayan crest during the formation of the ice dam.

Although regional damming appears to be more consistent with the existing data, we outline several unresolved issues with regard to this model:

(1) We have no direct evidence for the existence of an ice dam that is 1200 m above the current Yarlung River channel at the Zedong Gorge. This is because the thick (>500 m) moraine deposits at the wedge edge of the gorge were cut on top by a younger fluvial terrace surface.

(2) Although our combined analyses of zircon-grain zoning morphology and ages are consistent with the presence of Gangdese-sourced sediments in the inferred south-flowing fluvial system, we do not observe any granitic clasts that can be correlated unambiguously with the Gangdese Batholith north of the Yarlung River. It is unclear if this is a result of dilution (e.g., Zhang et al., 2012) and/or an extremely short duration of the inferred river diversion event.

(3) Although the terrace surfaces north and south of the Yarlung River are correlative in heights, the lack of age dating makes it uncertain whether the undated terraces north of the Yarlung River were developed synchronously with the dated terraces south of the Yarlung River. The lack of sedimentary studies on the valley-fill sediments north of the Yarlung River also prevents more detailed construction of the depositional processes and morphological development across the Woka basin north of the Yarlung River.

(4) There have been no reports, to our knowledge, on the presence of Quaternary lacustrine deposits at elevations >1200 m above the current Yarlung River, a requirement imposed by the regional damming model. On the hand, we are also not aware of any systematic search for such features along the Yarlung River valley directly west of the Zedong Gorge.

(5) The regional damming model predicts rapid sedimentation at a rate of ~76 mm/yr (i.e., deposition of ~1200 m thick sediments from ca. 24 k.y. B.P. to 8.2 k.y. B.P.). This rate seems excessively high when compared with the averaged erosional rate of ≤10 mm/yr across the eastern Himalaya and southeastern Tibet over a time scale of 5–10 m.y. (e.g., Zeitler et al., 2014; Tremblay et al., 2015). However, our rate is compatible with the sedimentation rate of ~87 mm/yr for the aggradational event induced by ice damming at the Yarlung Gorge, which deposited 680 m thick lacustrine sediments between 8.2 and 7.8 k.y. B.P. and 260 AD (Montgomery et al., 2004). The resultant high fluxes of sediments may have been related to both rapid glacier advances and high fluxes of hillslope-derived sediments as a result of increased pore pressure and higher frequency of landslides (Pratt et al., 2002). The latter may have caused sediment loads in the stream channels to exceed the fluvial transport capacity and thus caused riverbed aggradation and upward construction of fluvial terraces.

(6) The percentage of Cretaceous and Eocene zircon with an inferred Gangdese origin in valley-fill sediments is much lower than that determined from dating Yarlung River sand (Fig. 8). This may imply that the few Gangdese zircon grains may have been transported by wind across the Yarlung River, which would eliminate the need to appeal for the Siqunama-Yarlung connection to explain the deposition of valley-fill sediments in our study area.

The above issues highlight the need for further studies in the Yarlung drainage basin west of the Zedong Gorge. Specifically, a detailed investigation of the timing and depositional processes of valley fill in the Woka basin north of the Yarlung River will be critical for testing the validity of the regional damming model. In addition, a systematic investigation of the Quaternary sedimentary history along the main trunk of the Yarlung River west of the Zedong Gorge will also be critical in testing the two competing hypotheses.

CONCLUSIONS

The integrated results of our study led to the following conclusions.

(1) An aggradational event started at or after 24–20 k.y. B.P. and continued until or after 9.2–8.0 k.y. B.P. at the modern Himalayan drainage divide between the east-flowing Yarlung River and south-flowing Subansiri River in the eastern Himalaya. This event was associated with a major phase of glacier advance that filled up preexisting river valleys. The glacial valley fill was overlain by the deposition of a south-flowing fluvial sequence that lies across the Yarlung-Subansiri drainage divide.

(2) The timing of the recorded glacier advance correlates with the regional events of intense precipitation, rapid advances of alpine glaciers flowing down from rift-generated high peaks intersecting the local snow lines, and wide occurrence of ice damming along the main trunk and tributaries of the Yarlung River.

(3) Two possible models may explain the deposition of the aggradational sequence. First, an ice dam may have formed at a narrow gorge along the Siqunama River, which is controlled by an active rift zone. The ice dam was created by the advances of alpine glaciers from the nearby rift-bounding mountains intersecting the local snow lines. This model implies a limited northward shift (<40 km) of the current Yarlung-Subansiri drainage divide at 22–8.2 k.y. B.P. An alternative model is that the inferred ice dam jammed the Yarlung River at the western edge of the rift-induced Zedong Gorge. The dam caused the capture of the upper stream of the Yarlung River by the south-flowing Subansiri River.

(4) Although we are unable to differentiate the two competing models for the deposition of the aggradational sequence, our work indicates that combined climate change and tectonically induced topography have played a key role in controlling rapid shifts in drainage geometry at a time scale of <10 k.y. across the eastern Himalaya.

ACKNOWLEDGEMENTS

Detailed and highly constructive comments by the two journal reviewers have greatly improved the data description and final interpretations of this work. We gratefully acknowledge the support from the Tectonics Program, U.S. National Science Foundation, for this work in the eastern Himalaya. This project was also supported by a grant from SinoProbe-08 administered by the Chinese Academy of Geological Sciences and a grant from China University of Geosciences (Beijing). A careful review of an early draft of this paper and constructive suggestions made by Dave Montgomery and Noah Finnegan are greatly appreciated.

REFERENCES CITED

Adams, B.A., Hodges, K.V., Whipple, K.X., Ehlers, T.A., Soest, M.C., and Wartho, J., 2015, Constraints on the tectonic and landscape evolution of the Bhutan Himalaya from thermochronometry: Tectonics, v. 34, p. 1329–1347, doi:10.1002/2015TC003853.

Adlakha, V., Patel, R.C., and Lal, N., 2013, Exhumation and its mechanisms: a review of exhumation studies in the Himalaya: Journal of the Geological Society of India, v. 81, p. 481–502, doi:10.1007/s12594-013-0064-0.

Aikman, A.B., Harrison, T.M., and Ding, L., 2008, Evidence for early (>44 Ma) Himalayan crustal thickening, Tethyan Himalaya, southeastern Tibet: Earth and Planetary Science Letters, v. 274, p. 14–23, doi:10.1016/j.epsl.2008.06.038.

Aikman, A.B., Harrison, T.M., and Hermann, J., 2012a, Age and thermal history of Eo- and Neohimalayan granitoids, eastern Himalaya: Journal of Asian Earth Sciences, v. 51, p. 85–97, doi:10.1016/j.jseaes.2012.01.011.

Aikman, A.B., Harrison, T.M., and Hermann, J., 2012b, The origin of Eo- and Neo-himalayan granitoids, Eastern Tibet: Journal of Asian Earth Sciences, v. 58, p. 143–157.

Anderson, D.M., Overpeck, J.T., and Gupta, A.K., 2002, Increase in the Asian Southwest monsoon during the past four centuries: Science, v. 297, p. 596–599, doi:10.1126/science.1072881.

Armijo, R., Tapponnier, P., Mercier, J.L., and Han, T.L., 1986, Quaternary extension in southern Tibet: field observation and tectonic implications: Journal of Geophysical Research, v. 91, p. 13,803–13,872, doi:10.1029/JB091iB14p13803.

Attal, M., Tucker, G.E., Whittaker, A.C., Cowie, P.A., and Roberts, G.P., 2008, Modeling fluvial incision and transient landscape evolution: Influence of dynamic channel adjustment: Journal of Geophysical Research, v. 113, F03013, doi:10.1029/2007JF000893.

Benn, D., and Evans, D.J., 2014, Glaciers and glaciation: New York, Routledge, 802 p.

Benn, D.I., and Owen, L.A., 1998, The role of the Indian summer monsoon and the mid-latitude westerlies in Himalayan glaciation: review and speculative discussion: Journal of the Geological Society, v. 155, p. 353–363, doi:10.1144/gsjgs.155.2.0353.

Benn, D.I., and Owen, L.A., 2002, Himalayan glacial sedimentary environments: a framework for reconstructing and dating the former extent for glaciers in high mountains: Quaternary International, v. 97–98, p. 3–25, doi:10.1016/S1040-6182(02)00048-4.

Blair, T.C., and McPherson, J.G., 1994, Alluvial fans and their natural distinction from rivers based on morphology, hydraulic processes, sedimentary processes, and facies assemblages: Journal of Sedimentary Research, v. 64, p. 450–489.

Bracciali, L., Najman, Y., Parrish, R.R., Akhter, S.H., and Millar, I., 2015, The Brahmaputra tale of tectonics and erosion: Early Miocene river capture in the Eastern Himalaya: Earth and Planetary Science Letters, v. 415, p. 25–37, doi: 10.1016/j.epsl.2015.01.022.

Brookfield, M.E., 1998, The evolution of the great river systems of southern Asia during the Cenozoic India-Asia collision: Rivers draining southwards: Geomorphology, v. 22, p. 285–312, doi:10.1016/S0169-555X(97)00082-2.

Burg, J.P., Nievergelt, P., Oberli, F., Seward, D., Davy, P., Maurin, J.C., Diao, Z.Z., and Meier, M., 1998, The Namche Barwa syntaxis: evidence for exhumation related to compressional crustal folding: Journal of Asian Earth Sciences, v. 16, p. 239–252, doi:10.1016/S0743-9547(98)00002-6.

Burgess, W.P., Yin, A., Dubey, C.S., Shen, Z.K., and Kelty, T.M., 2012, Holocene shortening across the Main Frontal Thrust zone in the eastern Himalaya: Earth and Planetary Science Letters, v. 357–358, p. 152–167, doi:10.1016/j.epsl.2012.09.040.

Burns, S.J., Matter, A., Frank, N., and Mangini, A., 1998, Speleothem-based paleoclimate record from northern Oman: Geology, v. 26, p. 499–502, doi:10.1130/0091-7613(1998)026<0499:SBPRFN>2.3.CO;2.

Burrard, S.G., and Hayden, H.H., 1907, A Sketch of the Geography and Geology of the Himalaya Mountains and Tibet: Superintendent Government Printing, Calcutta, India.

Chauhan, O.S., 2003, Past 20,000-year history of Himalayan aridity: evidence from oxygen isotope records in the Bay of Bengal: Current Science, v. 84, p. 90–93.

Cina, S., Yin, A., Grove, M., Dubey, C.S., Shukla, D.P., Lovera, O.M., Kelty, T.K., Gehrels, G.E., and Foster, D.A., 2009, Gangdese arc detritus within the eastern Himalayan Neogene foreland basin: Implications for the Neogene evolution of the Yalu-Brahmaputra River system: Earth and Planetary Science Letters, v. 285, p. 150–162, doi: 10.1016/j.epsl.2009.06.005.

Clark, M.K., Schoenbohm, L.M., Royden, L.H., Whipple, K.X., Burchfiel, B.C., Zhang, X., Tang, W., Wang, E., and Chen, L., 2004, Surface uplift, tectonics, and erosion of eastern Tibet from large-scale drainage patterns: Tectonics, v. 23, TC1006, doi:10.1029/2002TC001402.

Clift, P.D., 2006, Controls on the erosion of Cenozoic Asia and the flux of clastic sediment to the ocean: Earth and Planetary Science Letters, v. 241, p. 571–580, doi:10.1016/j.epsl.2005.11.028.

Dodson, M.H., Compston, W., Williams, I.S., and Wilson, J.F., 1988, A search for ancient detrital zircons in Zimbabwean sediments: Journal of the Geological Society, v. 145, p. 977–983, doi:10.1144/gsjgs.145.6.0977.

Evans, D.J.A., Phillips, E.R., Hiemstra, J.F., and Auton, C.A., 2006, Subglacial till: formation, sedimentary characteristics and classification: Earth-Science Reviews, v. 78, p. 115–176, doi:10.1016/j.earscirev.2006.04.001.

Eyles, N., Eyles, C.H., and Miall, A.D., 1983, Lithofacies types and vertical profile models; an alternative approach to the description and environmental interpretation of glacial diamict and diamictite sequences: Sedimentology, v. 30, no. 3, p. 393–410, doi:10.1111/j.1365-3091.1983.tb00679.x.

Fleitmann, D., Burns, S.J., Mudelsee, M., Neff, U., Kramers, J., Mangini, A., and Matter, A., 2003, Holocene forcing of the Indian monsoon recorded in a stalagmite from Southern Oman: Science, v. 300, p. 1737–1739, doi: 10.1126/science.1083130.

Goodbred, S.L., and Kuehl, S.A., 2000, Enormous Ganges-Brahmaputra sediment discharge during strengthened early Holocene monsoon: Geology, v. 28, p. 1083–1086, doi:10.1130/0091-7613(2000)28<1083:EGSDDS>2.0.CO;2.

Goodsell, B., Hambrey, M.J., and Glasser, N.F., 2005, Debris transport in a temperate valley glacier: Haut Glacier d'Arolla, Valais, Switzerland: Journal of Glaciology, v. 51, no. 172, p. 139–146, doi:10.3189/172756505781829647.

Grujic, D., Coutand, I., Bookhagen, B., Bonnet, S., Blythe, A., and Duncan, C., 2006, Climatic forcing of erosion, landscape, and tectonics in the Bhutan Himalayas: Geology, v. 34, p. 801–804, doi:10.1130/G22648.1.

Gruszka, B., 2001, Climatic versus tectonic factors in the formation of the glaciolacustrine succession (Bełchatów outcrop, central Poland): Global and Planetary Change, v. 28, no. 1, p. 53–71, doi:10.1016/S0921-8181(00)00064-3.

Gupta, A.K., Anderson, D.M., and Overpeck, J.T., 2003, Abrupt changes in the Asian southwest monsoon during the Holocene and their links to the North Atlantic Ocean: Nature, v. 421, p. 354–356, doi:10.1038/nature01340.

Hallet, B., and Molnar, P., 2001, Distorted drainage basins as markers of crustal strain east of the Himalaya: Journal of Geophysical Research, v. 106, p. 13,697–13,709, doi: 10.1029/2000JB900335.

Hallet, B., Hunter, L., and Bogen, J., 1996, Rates of erosion and sediment evacuation by glaciers: A review of field data and their implications: Global and Planetary Change, v. 12, no. 1, p. 213–235, doi:10.1016/0921-8181(95)00021-6.

Harrison, T.M., Yin, A., Grove, M., Lovera, O.M., Ryerson, F.J., and Zhou, X., 2000, The Zedong Window: A record of superposed Tertiary convergence in southeastern Tibet: Journal of Geophysical Research, v. 105, p. 19,211–19,230, doi:10.1029/2000JB900078.

Hong, Y.T., Hong, B., Lin, Q.H., Zhu, Y.X., Shibata, Y., Hirota, M., Uchida, M., Leng, X.T., Jiang, H.B., Xu, H., Wang, H., and Yi, L., 2003, Correlation between Indian Ocean summer monsoon and North Atlantic climate during the Holocene: Earth and Planetary Science Letters, v. 211, p. 371–380, doi:10.1016/S0012-821X(03)00207-3.

Keller, E.A., Zepeda, R.L., Rockwell, T.K., Ku, T.L., and Dinklage, W.S., 1998, Active tectonics at Wheeler Ridge, southern San Joaquin Valley, California: Geological Society of America Bulletin, v. 110, no. 3, p. 298–310, doi:10.1130/0016-7606(1998)110<0298:ATAWRS>2.3.CO;2.

Korup, O., and Montgomery, D., 2008, Tibetan plateau river incision inhibited by glacial stabilization of the Tsangpo gorge: Nature, v. 455, p. 786–790, doi:10.1038/nature07322.

Korup, O., Montgomery, D.R., and Hewitt, K., 2010, Glacier and landslide feedbacks to topographic relief in the Himalayan syntaxes: Proceedings of the National Academy of Sciences of the United States of America, v. 107, p. 5317–5322, doi:10.1073/pnas.0907531107.

Kudrass, H.R., Hofmann, A., Doose, H., Emeis, K., and Erlenkeuser, H., 2001, Modulation and amplification of climatic changes in the Northern Hemisphere by the Indian summer monsoon during the past 80 ky: Geology, v. 29, p. 63–66, doi:10.1130/0091-7613(2001)029<0063:MAAOCC>2.0.CO;2.

Lang, K.A., and Huntington, K.W., 2014, Antecedence of the Yarlung-Siang-Brahmaputra River, eastern Himalaya: Earth and Planetary Science Letters, v. 397, p. 145–158, doi:10.1016/j.epsl.2014.04.026.

Lang, K.A., Huntington, K.W., and Montgomery, D.R., 2013, Erosion of the Tsongpo Gorge by megafloods, Eastern Himalaya: Geology, v. 41, p. 1003–1006, doi:10.1130/G34693.1.

Liang, Y.H., Chung, S.L., Liu, D.Y., Xu, Y.G., Wu, F.Y., Yang, J.H., Wang, Y.B., and Lo, C.H., 2008, Detrital zircon evidence from Burma for reorganization of the eastern Himalayan river system: American Journal of Science, v. 308, p. 618–638, doi:10.2475/04.2008.08.

Liu, W., Lai, Z., Hu, K., Ge, Y., Cui, P., Zhang, X., and Liu, F., 2015, Age and extent of a giant glacial-dammed lake at Yarlung Tsangpo gorge in the Tibetan Plateau: Geomorphology, v. 246, p. 370–376, doi:10.1016/j.geomorph.2015.06.034.

Liu, X.Q., Dong, H.L., Rech, J.A., Matsumoto, R., Yang, B., and Wang, Y.B., 2008, Evolution of Chaka Salt Lake in NW China in response to climatic change during the Latest Pleistocene-Holocene: Quaternary Science Reviews, v. 27, p. 867–879, doi:10.1016/j.quascirev.2007.12.006.

Ludwig, W., and Probst, J.L., 1998, River sediment discharge to the oceans; present-day controls and global budgets: American Journal of Science, v. 298, p. 265–295, doi: 10.2475/ajs.298.4.265.

Lupker, M., France-Lanord, C., Galy, V., Lavé, J., and Kudrass, H., 2013, Increasing chemical weathering in the Himalayan orogeny since the Last Glacial Maximum: Earth and Planetary Science Letters, v. 365, p. 243–252, doi: 10.1016/j.epsl.2013.01.038.

Matthes, F.E., 1972, Geologic history of the Yosemite Valley, *in* Embleton, C., ed., Glaciers and Glacial Erosion: Macmillan Education UK, p. 92–118.

McQuarrie, N., and Ehlers, T.A., 2015, Influence of thrust belt geometry and shortening rate on thermochronometer cooling ages: Insights from thermokinematic and erosion modeling of the Bhutan Himalaya: Tectonics, v. 34, p. 1055–1079, doi:10.1002/2014TC003783.

Miall, A.D., 1977, A review of the braided-river depositional environment: Earth-Science Reviews, v. 13, no. 1, p. 1–62, doi:10.1016/0012-8252(77)90055-1.

Miall, A.D., 1985, Architectural-element analysis: a new method of facies analysis applied to fluvial deposits: Earth-Science Reviews, v. 22, p. 261–308, doi:10.1016/0012-8252(85)90001-7.

Milliman, J.D., and Meade, R.H., 1983, World-wide delivery of river sediment to the oceans: The Journal of Geology, v. 91, p. 1–21, doi:10.1086/628741.

Montgomery, D.R., and Gran, K.B., 2001, Downstream variations in the width of bedrock channels: Water Resources Research, v. 37, p. 1841–1846, doi:10.1029/2000WR900393.

Montgomery, D.R., Hallet, B., Liu, Y.P., Finnegan, N., Anders, A., Gillespie, A., and Greenberg, H.M., 2004, Evidence for Holocene megafloods down the Tsangpo River gorge, southeastern Tibet: Quaternary Research, v. 62, p. 201–207, doi:10.1016/j.yqres.2004.06.008.

Neff, U., Burns, S.J., Mangini, A., Mudelsee, M., Fleitmann, D., and Matter, A., 2001, Strong coherence between solar variability and the monsoon in Oman between 9 and 6 kyr ago: Nature, v. 411, p. 290–293, doi:10.1038/35077048.

Owen, L.A., 2009, Latest Pleistocene and Holocene glacier fluctuations in the Himalaya and Tibet: Quaternary Science Reviews, v. 28, p. 2150–2164, doi:10.1016/j.quascirev.2008.10.020.

Owen, L.A., and Benn, D.I., 2005, Equilibrium-line altitudes of the Last Glacial Maximum for the Himalaya and Tibet: an assessment and evaluation of results: Quaternary International, v. 138–139, p. 55–78, doi:10.1016/j.quaint.2005.02.006.

Owen, L.A., Caffee, M.W., Finkel, R.C., and Seong, Y.B., 2008, Quaternary glaciation of the Himalayan-Tibetan orogeny: Journal of Quaternary Science, v. 23, p. 513–531, doi:10.1002/jqs.1203.

Pratt, B., Burbank, D.W., Heimsath, A., and Ojha, T., 2002, Impulsive alluviation during early Holocene strengthened monsoons, central Nepal Himalaya: Geology, v. 30, p. 911–914, doi:10.1130/0091-7613(2002)030<0911:IADEHS>2.0.CO;2.

Rhodes, E.J., 2011, Optically Stimulated Luminescence Dating of Sediments over the past 200,000 years: Annual Review of Earth and Planetary Sciences, v. 39, p. 461–488, doi:10.1146/annurev-earth-040610-133425.

Richardson, S.D., and Reynolds, J.M., 2000, An overview of glacial hazards in the Himalayas: Quaternary International, v. 65, p. 31–47, doi:10.1016/S1040-6182(99)00035-X.

Robinson, R.A.J., Brezina, C.A., Parrish, R.R., Horstwood, M.S.A., Oo, N.W., Bird, M.I., Thein, M., Walters, A.S., Oliver, G.J.H., and Zaw, K., 2013, Large rivers and orogens: The evolution of the Yarlung Tsangpo-Irrawaddy system and the eastern Himalayan syntaxis: Gondwana Research, doi:10.1016/j.gr.2013.07.002.

Ryan, W.B.F., Carbotte, S.M., Coplan, J.O., O'Hara, S., Melkonian, A., Arko, R., Weissel, R.A., Ferrini, V., Goodwillie, A., Nitsche, F., Bonczkowski, J., and Zemsky, R., 2009, Global multi-resolution topography synthesis: Geochemistry Geophysics Geosystems, v. 10, Q03014, doi: 10.1029/2008GC002332.

Santos, G.M., Southon, J.R., Druffel-Rodriguez, K.C., Griffin, S., and Mazon, M., 2004, Magnesium perchlorate as an alternative water trap in AMS graphite sample preparation: A report on sample preparation at KCCAMS at the Univ. of California, Irvine: Radiocarbon, v. 46, p. 165–173.

Schmidt, J.L., Zeitler, P.K., Pazzaglia, F.J., Tremblay, M.M., Shuster, D.L., and Fox, M., 2015, Knickpoint evolution on the Yarlung river: Evidence for late Cenozoic uplift of the southeastern Tibetan plateau margin: Earth and Planetary Science Letters, v. 430, p. 448–457, doi:10.1016/j.epsl.2015.08.041.

Schumm, S.A., and Khan, H.R., 1972, Experimental study of channel patterns: Geological Society of America Bulletin, v. 83, p. 1755–1770, doi:10.1130/0016-7606(1972)83[1755:ESOCP]2.0.CO;2.

Seeber, L., and Gornitz, V., 1983, River profiles along the Himalayan arc as indicators of active tectonics: Tectonophysics, v. 92, p. 335–367, doi:10.1016/0040-1951(83)90201-9.

Seward, D., and Burg, J.P., 2008, Growth of the Namche Barwa Syntaxis and associated evolution of the Tsangpo Gorge: Constraints from structural and thermochronological

data: Tectonophysics, v. 451, p. 282–289, doi:10.1016/j.tecto.2007.11.057.

Sharma, S., Joachimiski, M., Sharma, M., Tobschall, H.J., Singh, I.B., Sharma, C., Chauhan, M.S., and Morgenroth, G., 2004, Late glacial and Holocene environmental changes in Ganga plain, Northern India: Quaternary Science Reviews, v. 23, p. 145–159, doi:10.1016/j.quascirev.2003.10.005.

Sinha, A., Cannariato, K.G., Stott, L.D., Li, H.C., You, C.F., Cheng, H., Edwards, R.L., and Singh, I.B., 2005, Variability of Southwest Indian summer monsoon precipitation during the Bølling-Ållerød: Geology, v. 33, p. 813–816, doi:10.1130/G21498.1.

Snyder, N.P., Whipple, K.X., Tucker, G.E., and Merritts, D.J., 2000, Landscape response to tectonic forcing: Digital elevation model analysis of stream profiles in the Mendocino triple junction region, northern California: Geological Society of America Bulletin, v. 112, p. 1250–1263, doi:10.1130/0016-7606(2000)112<1250:LRTTFD>2.0.CO;2.

Stuiver, M., and Polach, H.A., 1977, Discussion: Reporting of C^{14} data: Radiocarbon, v. 19, p. 355–363.

Taylor, M., and Yin, A., 2009, Active structures of the Himalayan-Tibetan orogen and their relationships to earthquake distribution, contemporary strain field, and Cenozoic volcanism: Geosphere, v. 5, p. 199–214, doi:10.1130/GES00217.1.

Taylor, M., Yin, A., Ryerson, F.J., Kapp, P., and Ding, L., 2003, Conjugate strike-slip faulting along the Bangong-Nujiang suture zone accommodates coeval east-west extension and north-south shortening in the interior of the Tibetan Plateau: Tectonics, v. 22, 1044, doi:10.1029/2002TC001361.

Thompson, L.G., Yao, T., Davis, M.E., Henderson, K.A., Mosley-Thompson, E., Lin, P., Beer, J., Synal, H.A., Cole-Dai, J., and Bolzan, J.F., 1997, Tropical climate instability: The Last Glacial Cycle from a Qinghai-Tibetan ice core: Science, v. 276, p. 1821–1825, doi:10.1126/science.276.5320.1821.

Tremblay, M.M., Fox, M., Schmidt, J.L., Tripathy-Lang, A., Wielicki, M.M., Harrison, T.M., Zeitler, P.K., and Shuster, D.L., 2015, Erosion in southern Tibet shut down at ~10 Ma due to enhanced rock uplift within the Himalaya: Proceedings of the National Academy of Sciences of the United States of America, v. 112, no. 39, p. 12030–12035, doi:10.1073/pnas.1515652112.

Vermeesch, P., 2004, How many grains are needed for a provenance study?: Earth and Planetary Science Letters, v. 224, p. 441–451, doi:10.1016/j.epsl.2004.05.037.

Vermeesch, P., 2013, Multi-sample comparison of detrital age distributions: Chemical Geology, v. 341, p. 140–146, doi:10.1016/j.chemgeo.2013.01.010. (Corrigendum at http://dx.doi.org/10.1016/j.chemgeo.2013.12.009.)

Wang, P., Scherler, D., Liu-Zeng, J., Mey, J., Avouac, J.P., Zhang, Y., and Shi, D., 2014, Tectonic control of Yarlung Tsangpo Gorge revealed by a buried canyon in Southern Tibet: Science, v. 346, no. 6212, p. 978–981, doi:10.1126/science.1259041.

Wang, R.L., Scarpitta, S.C., Zhang, S.C., and Zheng, M.P., 2002, Later Pleistocene/Holocene climate conditions of Qinghai-Xizang Plateau (Tibet) based on carbon and oxygen stable isotopes of Zabuye Lake sediments: Earth and Planetary Science Letters, v. 203, p. 461–477, doi:10.1016/S0012-821X(02)00829-4.

Wang, X.L., Lu, Y.C., and Li, X.N., 2005, Luminescence dating of fine-grained quartz in Chinese loss-simplified multiple aliquot regenerative-dose (MAR) protocol: Dizhen Dizhi, v. 27, p. 615–622.

Webb, A.A.G., Yin, A., and Dubey, C.S., 2013, U-Pb zircon geochronology of major lithologic units in the eastern Himalaya: Implications for the origin and assembly of Himalayan rocks: Geological Society of America Bulletin, v. 125, p. 499–522, doi:10.1130/B30626.1.

Weissmann, G.S., Bennett, G.L., and Lansdale, A.L., 2005, Factors controlling sequence development on Quaternary fluvial fans, San Joaquin Basin, California, USA *in* Harvey, A.M., Mather, A.E., Stokes, M., eds., Alluvial Fans: Geomorphology, Sedimentology, Dynamics: Geological Society of London, Special Publication 251, p. 169–186, doi:10.1144/GSL.SP.2005.251.01.12.

Whittaker, A.C., Cowie, P.A., Attal, M., Tucker, G.E., and Roberts, G.P., 2007, Bedrock channel adjustment to tectonic forcing: Implications for predicting river incision rates: Geology, v. 35, p. 103–106, doi: 10.1130/G23106A.1.

Xie, L.W., Zhang, Y.B., Zhang, H.H., Sun, J.F., and Wu, F.Y., 2008, In situ simultaneous determination of trace elements, U-Pb and Lu-Hf isotopes in zircon and baddeleyite: Chinese Science Bulletin, v. 53, p. 1565–1573.

Yao, T., Thompson, L., Yang, W., Yu, W., Gao, Y., Guo, X., Yang, X., Duan, K., Zhao, H., Xu, B., and Pu, J., 2012, Different glacier status with atmospheric circulations in Tibetan Plateau and surroundings: Nature Climate Change, v. 2, no. 9, p. 663–667, doi:10.1038/nclimate1580.

Yin, A., 2000, Mode of Cenozoic east-west extension in Tibet suggesting a common origin of rifts in Asia during the Indo-Asian collision: Journal of Geophysical Research, v. 105, B9, p. 21745–21759, doi:10.1029/2000JB900168.

Yin, A., 2006, Cenozoic tectonic evolution of the Himalayan orogen as constrained by along-strike variation of structural geometry, exhumation history, and foreland sedimentation: Earth-Science Reviews, v. 76, p. 1–131, doi:10.1016/j.earscirev.2005.05.004.

Yin, A., 2010, Cenozoic tectonic evolution of Asia: A preliminary synthesis: Tectonophysics, v. 488, p. 293–325, doi:10.1016/j.tecto.2009.06.002.

Yin, A., Harrison, T.M., Ryerson, F.J., Chen, W.J., Kidd, W.S.F., and Copeland, P., 1994, Tertiary structural evolution of the Gangdese thrust system, southeastern Tibet: Journal of Geophysical Research, v. 99, B9, p. 18175–18201, doi:10.1029/94JB00504.

Yin, A., Harrison, T.M., Murphy, M.A., Grove, M., Nie, S., Ryerson, F.J., Wang, X.F., and Chen, Z.L., 1999, Tertiary deformation history of southeastern and southwestern Tibet during the Indo-Asian collision: Geological Society of America Bulletin, v. 111, p. 1644–1664, doi:10.1130/0016-7606(1999)111<1644:TDHOSA>2.3.CO;2.

Yin, A., Dubey, C.S., Kelty, T.K., Gehrels, G.E., Chou, C.Y., Grove, M., and Lovera, O.M., 2006, Structural evolution of the Arunachal Himalaya and implications for asymmetric development of the Himalayan orogeny: Current Science, v. 90, p. 195–206.

Yin, A., Dubey, C.S., Kelty, T.K., Webb, A.A.G., Harrison, T.M., Chou, C.Y., and Célérier, J., 2010, Geological correlation of the Himalayan orogen and Indian craton: Part 2. Structural geology, geochronology, and tectonic evolution of the eastern Himalaya: Geological Society of America Bulletin, v. 122, p. 360–395, doi:10.1130/B26461.1.

Zeitler, P.K., Koons, P.O., Bishop, M.P., Chamberlain, C.P., Craw, D., Edwards, M.A., Hamidullah, S., Jan, M.Q., Khan, M.A., Khattak, M.U.K., Kidd, W.S.F., Mackie, R.L., Meltzer, A.S., Park, S.K., Pecher, A., Poage, M.A., Sarker, G., Schneider, D.A., Seeber, L., and Shroder, J.F., 2001, Crustal reworking at Nanga Parbat, Pakistan: Metamorphic consequences of thermal mechanical coupling facilitated by erosion: Tectonics, v. 20, p. 712–728, doi:10.1029/2000TC001243.

Zeitler, P.K., Meltzer, A.S., Brown, L., Kidd, W.S.F., Lim, C., and Enkelmann, E., 2014, Tectonics and topographic evolution of Namche Barwa and the easternmost Lhasa Block, Tibet, *in* Nie, J., Horton, B.K., and Hoke, G.D., eds., Toward an Improved Understanding of Uplift Mechanisms and the Elevation History of the Tibetan Plateau: Geological Society of America Special Paper 507, p. 23–58, doi:10.1130/2014.2507(02).

Zeng, L.S., Gao, L.E., Xie, K.J., and Liu, J., 2011, Mid-Eocene high Sr/Y granites in the northern Himalayan gneiss domes: Melting thickened lower continental crust: Earth and Planetary Science Letters, v. 303, p. 251–266, doi:10.1016/j.epsl.2011.01.005.

Zhang, D.D., 2001, Tectonically controlled fluvial landforms on the Yaluzangbu River and their implications for the evolution of the river: Mountain Research and Development, v. 21, p. 61–68, doi:10.1659/0276-4741(2001)021[0061:TCFLOT]2.0.CO;2.

Zhang, J.Y., Yin, A., Liu, W.C., Wu, F.Y., Ding, L., and Grove, M., 2012, Coupled U-Pb dating and Hf isotopic analysis of detrital zircon of modern river sand from the Yalu River (Yarlung Tsangpo) drainage system in southern Tibet: Constraints on the transport processes and evolution of Himalayan rivers: Geological Society of America Bulletin, v. 124, p. 1449–1473, doi:10.1130/B30592.1.

Zhang, P., Shen, Z., Wang, M., Gan, W., Burgmann, R., and Molnar, P., 2004, Continuous deformation of the Tibetan Plateau from global positioning system data: Geology, v. 32, p. 809–812, doi:10.1130/G20554.1.

Zhao, Z.D., Mo, X.X., Guo, T.Y., Zhou, S., Dong, G.C., Wang, L.L., Zhang, F.Q., and Wan, J.L., 2003, Apatite Fission Track Ages for southern Tibetan batholiths and the uplift of Tibetan Plateau: Science Progress, v. 13, p. 877–880.

MANUSCRIPT RECEIVED 23 SEPTEMBER 2015
REVISED MANUSCRIPT RECEIVED 21 MARCH 2016
MANUSCRIPT ACCEPTED 18 APRIL 2016

Printed in the USA